

**Electron Generations and Transportation
in Fast Ignition Experiments**

Sehar Sarfraz

**A thesis submitted for the degree of
Master of Science**

**University of York
Department of Physics**

July 2011

Abstract

This thesis described the generation and transportation of hot electron in fast ignition experiments. A brief review of the background and the theory of inertial confinement fusion process are discussed. This thesis explains different schemes of fast ignition alongside the various relevant electron energy spectrum diagnostic techniques. The experiment was performed using the Vulcan PetaWatt laser at the Rutherford Appleton Laboratory. Capsules in which a re-entrant gold cone has been imbedded were involved in the experiment as targets. Gold cone targets, with a wall thickness of 20 μm and a tip thickness of 6 μm were used in the experiment. Each cone had a 40 μm diameter, approximately 1mm long copper wire attached to its tip. An electron spectrometer was used which was aligned along the axis of the wire attached to the gold cone. Results of the experiment explained the electron energy spectrum in a high energy picosecond 1.053 μm laser pulse interaction with a cone-wire target, with various degrees of laser defocusing. Diagnostics also included electron energy spectra with electron energies between 1MeV to 8MeV using image plates as detectors and found the relevant relativistic maxwellian temperature for each energy curve associated with different targets and with a different degree of laser defocusing. The results show that with an increase of defocusing of the laser, energy coupling remains the same in the cone while softening the electron energy.

Contents

Acknowledgements 6

Declaration 8

Chapter 1

1.0 Inertial Confinement Fusion 9

1.1 Introduction 10

1.2 Nuclear fusion 14

1.3 Confinement of fuel 19

1.4 Basic process of Inertial Confinement Fusion 21

1.5 Schemes for Inertial confinement fusion 27

1.5.1 Indirect drive 27

1.5.2 Direct drive implosion 31

1.6 Central hotspot vs. Fast Ignition 33

1.7 References 34

Role of the Author 37

Chapter 2

2.0 Fast Ignition 38

| | |
|---|-----------|
| 2.1 Hole-boring scheme or self-focusing scheme | 43 |
| 2.2 Cone-guided fast ignition | 47 |
| 2.3 Hot electron generation and transportation in short pulse laser-solid target interaction | 50 |
| 2.4 Ponderomotive acceleration | 52 |
| 2.5 Ohmic inhibition and heating | 52 |
| 2.6 Reference | 54 |

Chapter 3

| | |
|--|-----------|
| 3.0 Electron Spectroscopy | 56 |
| 3.1 K-α diagnostics | 61 |
| 3.1.1 HOPG Spectrometer | 61 |
| 3.1.2 Cu K-α crystal imager | 62 |
| 3.2 Single Hit CCD | 62 |
| 3.3 Electron spectrometer | 62 |
| 3.4 Image Plates (IP) | 65 |
| 3.5 References | 67 |

Chapter 4

| | |
|---------------------------------|-----------|
| 4.0 Results and analysis | 69 |
| 4.1 Data Analysis | 69 |
| 4.2 Results | 72 |
| 4.3 Summary of results | 82 |
| 4.4 References | 86 |

Chapter 5

| | |
|------------------------|-----------|
| 5.0 Conclusions | 87 |
| 5.1 References | 89 |

List of Figures

| | |
|---|-----------|
| Figure 1.1. World's energy consumption sources. | 10 |
| Figure 1.2. Energy consumption per capita | 12 |
| Figure 1.3. Binding energy per nucleon | 16 |
| Figure 1.4. Reaction rate | 18 |
| Figure 1. 5 Central hot spot scheme's fuel configuration, | 23 |
| Figure 1.6. The Rayleigh-Taylor instability | 26 |
| Figure 1.7. NIF target pellet inside a hohlraum capsule, | 29 |
| Figure 1.8. Indirect drive sequence | 30 |
| Figure 1.9. Central hot spot inertial confinement fusion | 32 |
| Figure 2.1. Difference between the two schemes for hot spot generation | 41 |
| Figure 2.2. Isobaric and Isochoric compression | 42 |
| Figure 2.3. Laser hole boring scheme | 46 |
| Figure 2.4. Cone guided target | 48 |
| Figure 2.5. Fast ignition target | 49 |
| Figure 3.1. The gold cone and the wire attached to the cone | 59 |

| | |
|--|--------------|
| Figure 3.2 the Chamber setup | 60 |
| Figure3.3.Electron septrometer | |
| 64 | |
| Figure 4.1. Shows the raw (QL) data stored on image plate | 70 |
| Figure 4.2. to 4.17. Results | 73-81 |
| Figure 4.18. Hot electron slop | 82 |
| Figure 4.19. Variation of the length over which the K_{α} emission falls to $1/e$ of its peak value in the same. | 83 |

Acknowledgements

First of all would like to thank all mighty GOD for providing me such a knowledgeable opportunity to excel myself. I would like to gratefully and sincerely thank **Dr. John Pasley** for his guidance, understanding, patience, and most importantly, his friendship during my graduate studies and for everything you have done for me. I also would like to pay my gratitude towards those who have provided me a well rounded experience consistent my long-term career goals; those who have encouraged me to not only grow as an experimentalist but also as an independent thinker. I am not sure many graduates are given the opportunity to develop their own individuality and self-sufficiency by being allowed to work with such independence.

I would also like to thank **Louren Hobbs** for their constant help, support and guidance throughout this study. I also would like to thank her for providing me with much experimental information and data from this particular study. She also helped me as a friend to understand the culture and environment, so that I could adjust myself properly to it.

I also would like to thank all the academic and technical staff of the Physics department for their constant support and help. I also would like to show my

gratitude to the computing and library staff of the University of York for providing me with the best environment and services throughout my research.

My parents Mr & Mrs Sarfraz Hussain, deserve my special thanks for the excellent educational foundation that they laid for me with much love and care, many years ago. I would like to thank my brother Amad and my sister Sakina for their moral support.

Finally I thank everyone who in one way or the other contributed in his or her small way to help me complete this course of study and present this study in its present form.

God Bless You All.

Declaration

I declare that the work submitted in this thesis is based on the result of my own investigation, unless otherwise stated. It has not been submitted for any degree in this or any other university and is not submitted simultaneously to another level.

Sehar Sarfraz

22/7/11

Chapter 1

1.0 Inertial Confinement Fusion

Energy and life have always being interconnected. Finding new sources of energy is a key pursuit for this current generation. Implementing new, cost-effective and clean sources of energy would not only support the present population of the world but would also be hugely beneficial for future generations. These issues are not only important for scientists, but are also widely discussed in a socio-economic and political context. Scientists all over the world are striving to develop new energy sources which will not be the depleted [1].

1.1 Introduction

The sun was the only source of energy for the first five to ten million years of human existence. However the growing needs of the man led him to find different sources of energy. Starting from the first manmade fires, we have tried to develop increasingly sophisticated sources of energy [2].

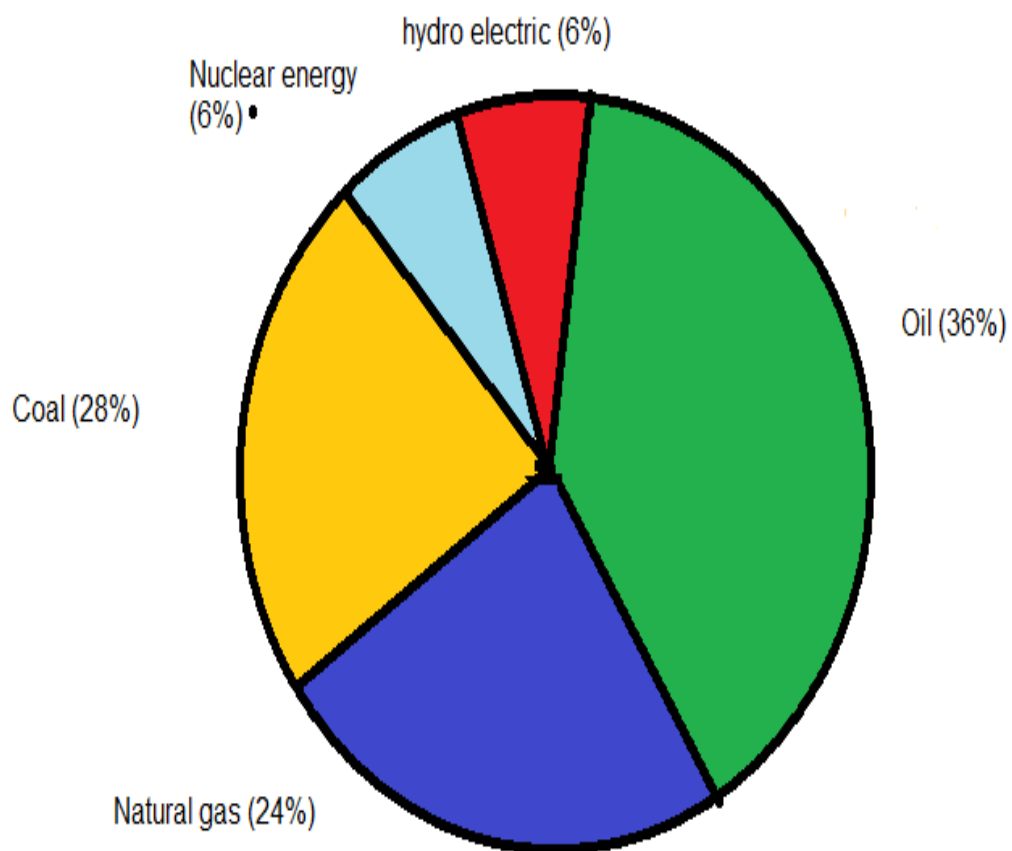


Figure 1.1. World's energy consumption sources. It shows fossil fuels fulfil 88% of the world's energy consumption needs. Only 12% of energy is produced by other sources [3].

Currently 88% of the world's energy source production and consumption is in the form of fossil fuels as show in figure 1.1 which is based on a survey done in 2006 in Canada [3]. Fossil fuels are appealing as a source of energy due to their ability to be converted to commercial power with high efficiency. However there are many issues related to this kind of energy source. Fossil fuels are non-renewable. If the world's nations keep consuming energy at the present rate then oil and gas will only provide energy for approximately the next 100 years; coal for approximately for the next 200 years [4].

The world's population is increasing and the societies are always looking for a better and more sophisticated lifestyle [4]. This increases the energy consumption per capita. It increases the energy demand on a year-to-year basis, as shown in the figure 1.2, which shows energy consumption per capita from 1925 to 2005 [5].

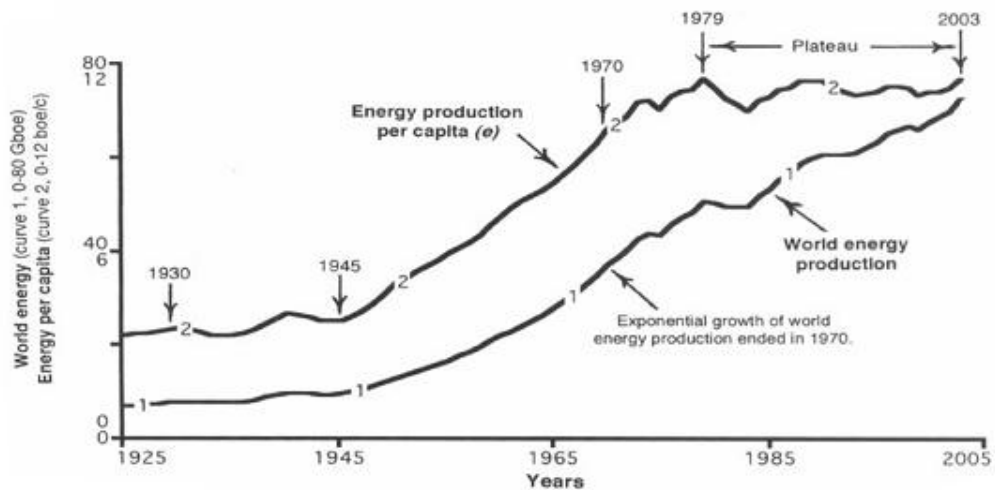


Figure 1.2. Energy consumption per capita and total global energy production from 1925 to 2005 [5] .

This energy consumption rate is shrinking the inventory of fossil fuels faster ever more rapidly. Figure 1.2 suggests that, in the light of a swelling global population, global energy demands are not likely to diminish in the near term [5].

The scientific community is working to develop alternative energy sources, which are both renewable and low in cost, such as hydro, wind and solar. The utility of these alternative energy sources depends strongly upon on our ability to convert them efficiently into commercial electricity. However the combined contribution of such alternative energy sources is only approximately 7-8% of the total world production. In addition, while fossil fuels can easily be transported to any location, some of these alternative energy sources are highly

dependent upon the local geography and climate. This can limit their utility in many cases [5].

Another issue which has forced us to think about alternative energy sources is that of the production of harmful gases released during the combustion of fossil fuels. CO₂ is released as a major combustion product which pollutes the environment. A report based on a research done by the US Department of Energy and Environment Protection Agency shows that due to the combustion of fossil fuels millions of tons of CO₂ has been released in atmosphere in the past 150 years. According to this report, in 1999 alone almost 2.5 million tons of CO₂ were been released into our earth's atmosphere [6]. The presence of CO₂ in the earth's atmosphere at greater than normal concentrations causes a range of problems such as global warming and the greenhouse effect [7].

These considerations have resulted in the scientific community focussing efforts upon developing alternative sources of energy which are renewable, efficiently converted in commercial power and have less damaging effects upon the environment. This led them to the idea of using nuclear fission energy as an alternative to fossil fuel. In late 1940s and early 1950s, nuclear reactors were used for the 1st time to generate commercial electricity. Many considered this to be a key solution to the world's energy crises. Fission can readily replace fossil fuel burning power reactors. However there are problems related to the production of fission waste products. The radiation emitted from these fission daughter nuclides and their descendants would have devastating effects upon the environment were they to be released. This has created much controversy,

both in terms of the safety of such reactors, and also in terms of the methods and locations of transportation and storage of the radioactive waste products [8].

This analysis of current world energy supply and demand, casts a seemingly grim outlook for future generations. However, one promising energy source remains for which a strong case can be made: nuclear fusion energy.

1.2 Nuclear fusion

Fusion is a natural phenomenon which has been present in nature since the earliest epochs, as the process which fires the stars. The sun provides light and energy to our world; energy from nuclear fusion. In the early 1930s scientists were able to perform a fusion experiment on earth for the first time [9]. Now they are trying to achieve self-sustained fusion reactions in a fusion reactor to produce electricity [10].

The physics behind fusion is relatively straightforward. It is a process that occurs between two atomic nuclei. Nuclei are positively charged and have strong repulsive forces which prevent them from readily moving closer together. The nuclei must have a high energy in order to overcome this constraint and fuse together to form the fusion products which are always of slightly lower mass than the reactant nuclei [11].

The strong nuclear force is a short range attractive force that tends to bind the nuclei together. As the nuclei are positively charged they must have sufficient kinetic energy to overcome their mutual Coulomb repulsion. If they are able to do this, then the strong nuclear force may bind the nuclei together into a lower potential state, releasing energy in this process. The energy released in fusion is equivalent to the difference in mass of the reactant and product nuclei. The energy released is distributed amongst the fusion products, so as to conserve energy and momentum [11]. This energy released can be calculated from Einstein's famous mass-energy equivalency relationship [12], $E=mc^2$.

The viability of a fusion reaction (whether it is endothermic or exothermic) is determined by a consideration of the curve of the binding energy of the nucleons. Binding energy per nucleon is plotted in figure 1.3.

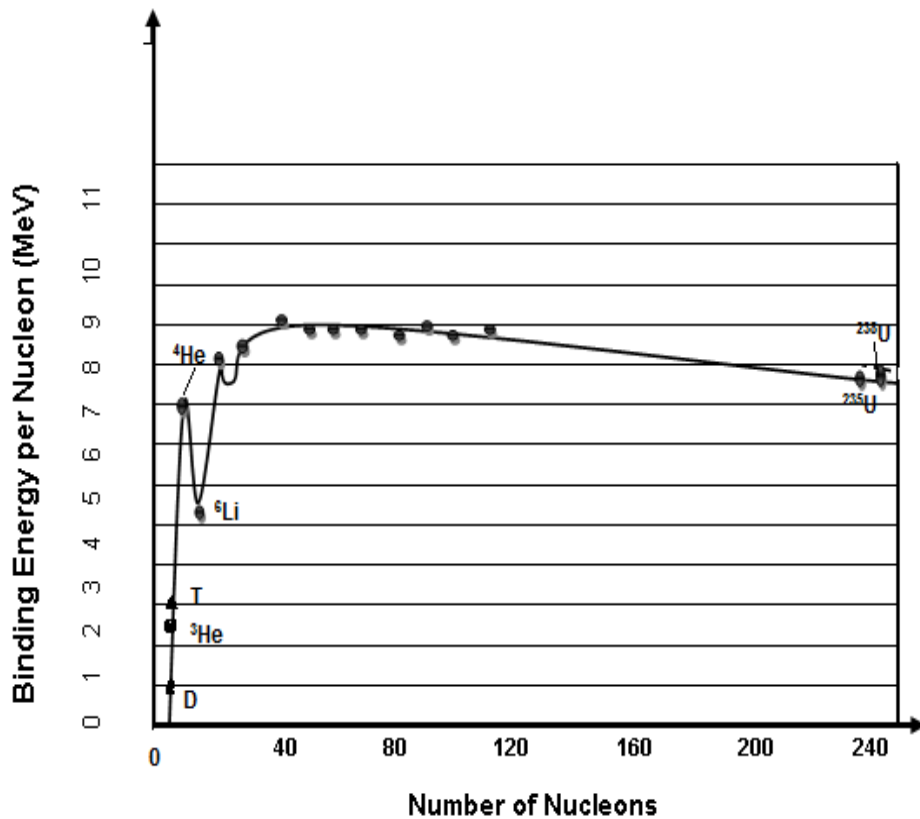


Figure 1.3. Binding energy per nucleon is explained in the above figure. Binding energy curve more appropriate for fusion reaction as the energy required to fuse to nuclei is low in that case [11].

The hydrogen isotopes deuterium (D) and tritium (T) have the lowest binding energy per nucleon. The tendency for the binding energy to decrease with increasing nuclear mass above iron implies that, for heavier nuclei, fission rather than fusion will be energetically favoured (and therefore fusion does not occur for heavy elements).

For the Deuterium–Tritium reaction:



The repulsion energy associated with the Coulomb force between the deuterium and tritium nuclei is 370keV; however quantum tunnelling allows fusion reactions to occur at lower energies [11], [13].

The probability of a fusion reaction occurring depends strongly upon the temperature of the fuel. From comparatively low temperatures, the fusion cross section increases with increasing temperature, until it reaches a maximum value, at a temperature of many hundreds of millions or billions of Kelvin (depending on the reaction being considered). As can be seen from figure 1.4, the DT reaction cross-section, peaks at a relatively low temperature of around 70keV [11], [13], [14].

For the D-T fuel the cross section is several orders of magnitude higher than for other fuels at low temperatures. This fact makes it a best fuel choice for fusion reactors [14], as even raising fusion fuel to “low” temperatures, on these scales, is exceptionally challenging. The threshold temperature for the D-T reaction is 5-10keV, which is very small compared to other reactions [15], [16].

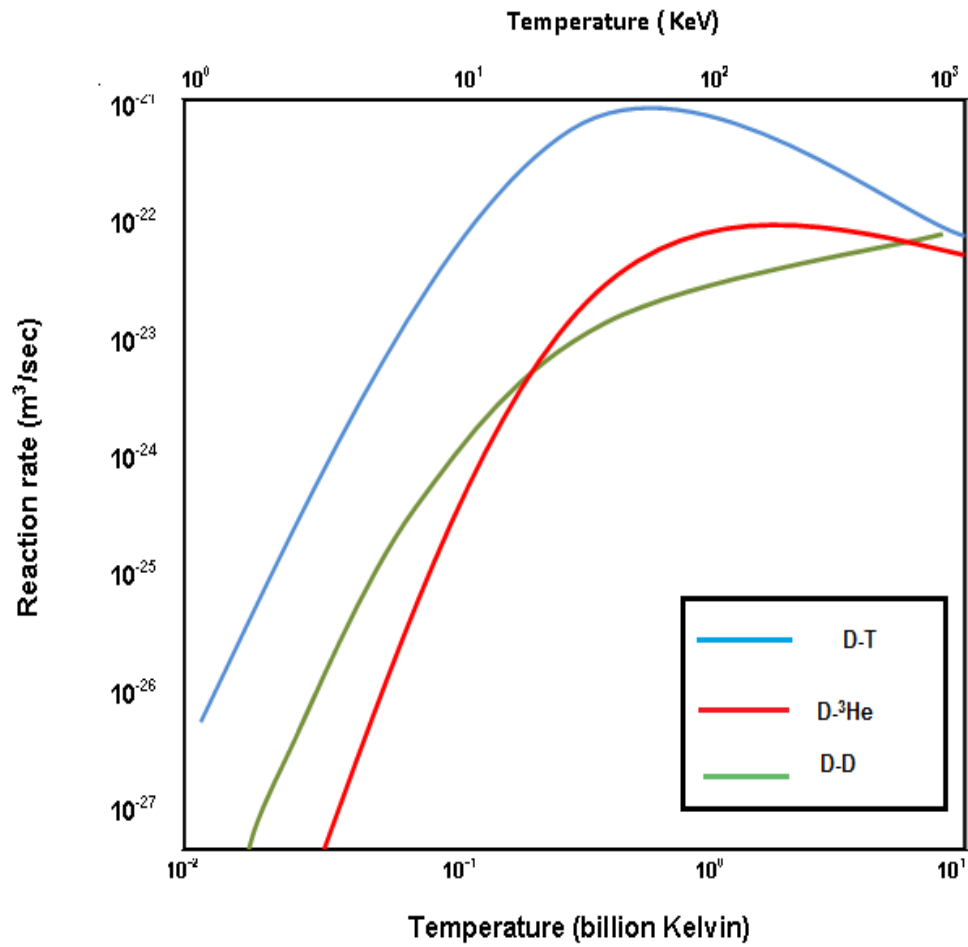


Figure 1.4. Reaction rate. [13]. This figure shows that the Maxwellian-averaged D-T cross section is several orders of magnitude higher than for other fuels at low temperatures. In addition, the threshold temperature for the D-T reaction is 5-10keV, which is very small compared to other reactions as we can see from the diagram.

1.3 Confinement of fuel

Historically the major obstacle to fusion energy is that the temperatures required in order to achieve fusion prohibits the use of a confinement vessel in which the fuel is in direct contact with the vessel walls. This then raises the question: how can the fuel be contained, if not by a containment vessel which is in contact with the fuel? [11], [12].

Two key schemes have been proposed for fusion. Both of these schemes satisfy the power balance equations published by J.D. Lawson in 1957 [15]. These constraints are known as the Lawson criteria. According to Lawson, the α -particle energy deposition from the D-T reaction must be sufficient to maintain the temperature of the burning plasma against all the loss mechanisms. The reaction cools down due to radiative and conductive heat loss [16], [16]. Furthermore, in order to be viable from a fusion energy perspective, the fuel must be confined for long enough that more energy is released than was required to heat the fuel to the point of ignition [18]. The Lawson criterion, which sets the boundary conditions for viable fusion energy release, is stated as $n_e \tau \geq 1.5 \times 10^{20} \text{s/m}^3$ where n_e is the electron number density per cubic metre and τ is the plasma confinement time in s. The precise minimum value of the product required for viable fusion is dependent upon the burn temperature; the minimum of $\sim 1.5 \times 10^{20} \text{s/m}^3$ being reached at a burn temperature of around 25keV.

The first apparently viable confinement scheme was proposed in 1951. This employs magnetic fields to confine the fuel, and is therefore referred to as Magnetic Confinement Fusion (MCF). MCF is a fusion process where the plasma particles are constrained to move along the magnetic field lines. The ITER tokamak is a toroidally shaped reactor which uses close field geometry [17]. The magnetic field lines form rings around the toroid. Plasma particles move along these orbital field lines and remain confined, thereby avoiding contact with the walls. In this type of fusion process strong magnetic fields are used to confine low density plasma ($\sim 10^{14} \text{ cm}^{-3}$) for long periods of time (many seconds or minutes) [19], [18].

In 1960 the first laser was constructed. The idea of achieving fusion ignition with lasers was proposed by John Nuckolls a few weeks after the laser was first invented, although the idea was not published openly until 1972 [13]. This approach to fusion is called inertial confinement fusion (ICF) because there is no external force applied to confine the fuel; Lawson's criteria is satisfied by the confinement that results from the fuel's own inertia [11].

ICF relies upon the burn rate in highly compressed fuel being sufficient that sufficient energy is released in the time over which the inertia keeps the fuel together. Fuel can be compressed to very high densities, more than 1000 times the original density of the fuel by the application of intense radiation in the ICF scheme [19]. The fusion reaction rate increases with the square of the fuel density [21]. This enables the scheme to satisfy Lawson's criteria, even though

the time scale of the fusion burn may only be a few tens of picoseconds [15], [26].

1.4 Basic process of Inertial Confinement Fusion

In spite of a number of variations on the scheme since it was first published in 1972, the essentials of the inertial confinement fusion process remain the same now as they did then. Fuel is compressed by energetic beams to achieve the required densities and temperatures for ignition [22].

In ICF the DT fuel is contained in a small spherical fuel capsule, on the order of a millimetre in radius. This consists of three regions, a low atomic number surface region, known as the ablator, a layer of solid DT-ice fuel, and then, occupying most of the volume, a central region of DT gas. For a typical ICF implosion the target will undergo four phases, the first two of which occur concurrently: ablation, compression, ignition and burn [23]. The ICF capsule is symmetrically irradiated by a driver which can be a laser, X-rays or ion beams [20]. The outer surface of the fuel capsule heats up and ablates outward. The surface heating also generates shock waves which propagate inward, accelerating the shell in what can be seen as a rocket-like reaction to the ablative expansion of the outermost layers of the capsule. A number of spherically symmetric shocks must be launched in order to achieve high compression. The shocks are carefully timed in order to keep the fuel at low entropy; excessive fuel entropy limits compression. The fuel typically implodes over a period of several tens of

nanoseconds, finally reaching extreme densities. The increasing pressure in the central region causes the shell implosion to stagnate. At the time of stagnation the central region comes into pressure equilibrium with the shell that is imploding around it: the pressure exerted by the hot central region comes to balance that of the much colder, denser imploding fluid. The compressive heating of the central region by the surrounding shell results in the formation of a hotspot at the centre of the fuel, and it is in this region that the ignition occurs [11], [20]. If a uniform implosion is achieved, a compressed fuel profile much like that shown in figure1.5 is attained.

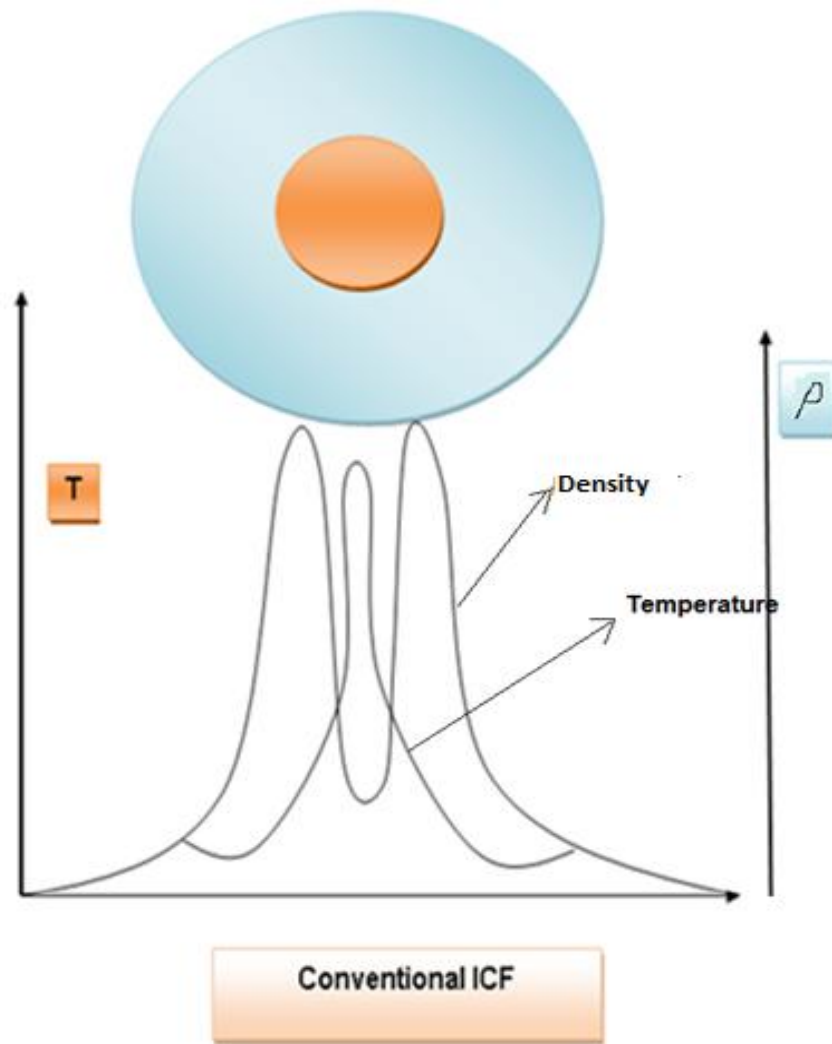


Figure 1.5. shown here is the central hot spot scheme's fuel configuration, density (ρ) and temperature (T) profile of a conventional central hot spot inertial confinement fusion target [21].

The sequence of shock waves and compression heats the central gas fill from around 500eV to 10keV in the final few hundred picoseconds of the implosion. This exceeds the threshold temperature for ignition in the DT mixture [11], [12]. These temperatures, achieved by compression, are high enough to start the ignition process. Alpha particles and neutrons are generated in this hot region of DT plasma. The overwhelming majority of the neutrons escape from the surface

of the target without depositing a significant fraction of their energy [17]. The range of alpha particles is very small [11] $0.3\text{g}/\text{cm}^2$ however, and so these are likely to be stopped by the surrounding fuel and redeposit their energy into the hot spot, provided that the hotspot density-radius product is somewhat greater than the alpha particle range. This results in self-heating of the hotspot, otherwise known as boot-strapping [18], [20]. The further heating results in enhanced alpha particle production, and further heating, until the hotspot is burning violently. Burn can then spread into the surrounding dense fuel. Capsules proposed for power production may produce gains in excess of one hundred and yields of hundreds of Mega-Joules, the key to high gain being that the bulk of the fuel heating is performed by the propagating burn wave rather than by the driver [17], [22].

A major challenge to the successful implosion of an ICF capsule is the Rayleigh-Taylor instability (RTI). Non-uniform irradiation or a non-uniform target surface will result in the growth of the Rayleigh Taylor instability. This is the instability which occurs when a light fluid pushes on, or supports, a denser fluid, resulting in characteristic bubble and spike growth at the interface. The Rayleigh-Taylor instability can potentially inhibit the successful formation of the central hotspot/surrounding dense fuel configuration previously described [17].

Rayleigh-Taylor instabilities may grow during two distinct phases of an ICF implosion:

1. During the acceleration phase, when the driver interacts with the outer surface of the target. The pressure peak lies in material that is less dense than that which is being driven inward- so the configuration is Rayleigh-Taylor unstable [11], [17], [20].
2. At the end of the implosion, these instabilities can grow at the interface between the dense fuel and the hotspot, when the less dense material is decelerating the surrounding denser fuel that is imploding into it [11].

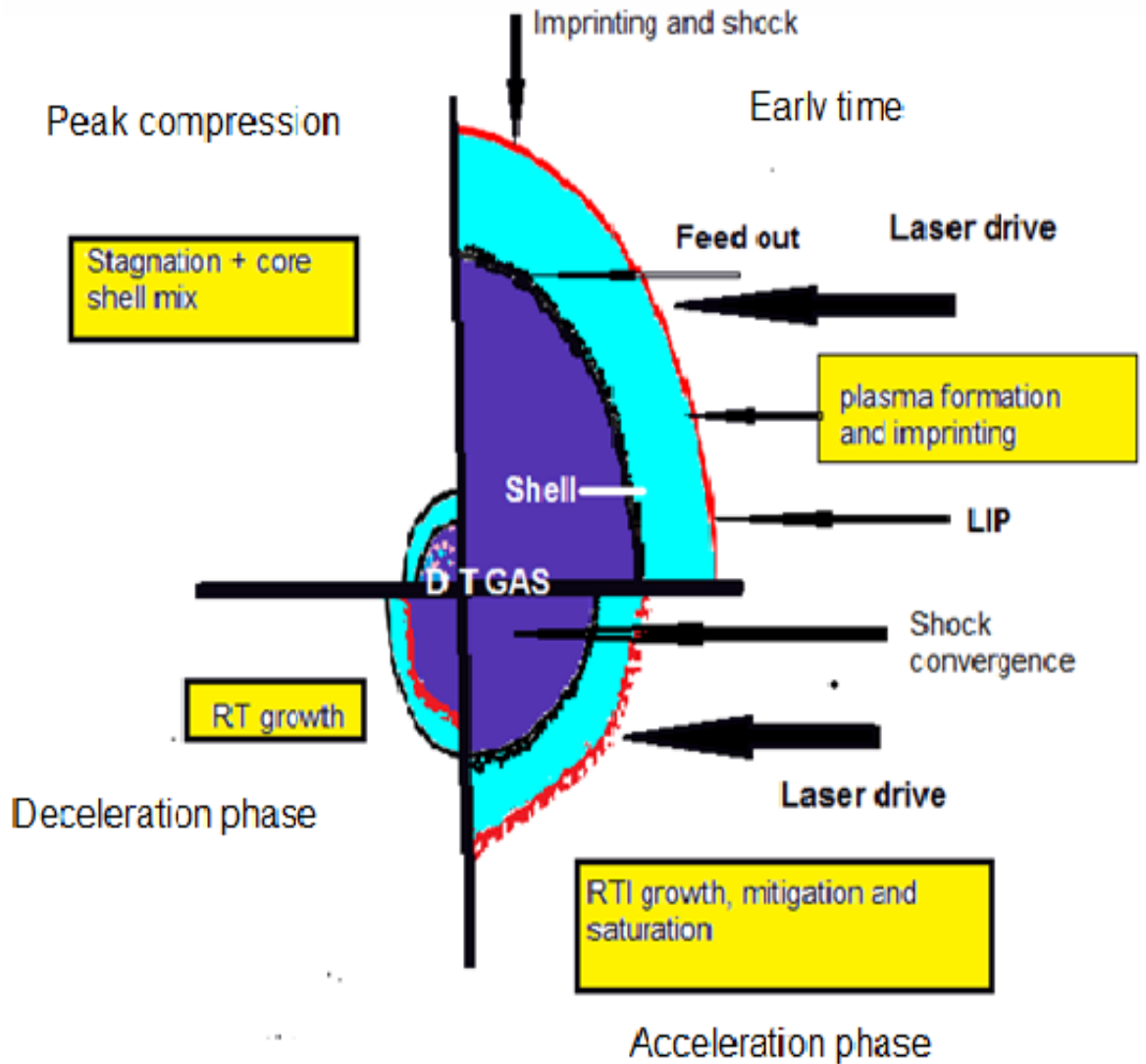


Figure 1.6. The Rayleigh-Taylor instability occurs at the outer shell surface in the acceleration phase and at the inner surface in the deceleration phase. The instability can lead to shell breakup and quenching of the fusion burn by mixing of the cold shell material and the heated DT gas [22].

The thickness of the fuel shell relative to the overall capsule radius is an important ratio in regard to maintaining the integrity of the fuel during the implosion process [11]. Excessively thin fuel layers tend to be insufficiently

robust to survive disruption by the RTI. So, in addition to ensuring a uniform drive, and capsule surface, the ICF capsule designer also has some freedom to make a capsule more robust to the RTI by increasing the fuel layer thickness relative to the overall capsule radius [10].

1.5 Schemes for Inertial confinement fusion

Two distinct schemes are employed in inertial confinement fusion, direct and indirect drive. With direct drive, the laser or particle beam driver is applied directly to the fuel capsule surface. In the case of indirect drive, however, the driver energy is first converted into thermal x-rays, and it is these x-rays which drive the implosion [17], [21]. We shall consider each of these two schemes in a little more detail.

1.5.1 Indirect drive

In this scheme, the ablation of the fuel target is driven by thermal radiation emitted by the walls of a cavity, otherwise known as a hohlraum, rather than being illuminated directly by energetic laser beams (or other directed radiation sources) [11].

The target capsule is suspended within the “hohlraum”. The walls of this cavity are in an approximate state of equilibrium with the radiant energy in the void

regions of the cavity. The hohlraum is typically cylindrically symmetric, with the capsule placed centrally, and laser beams emerging from laser entrance holes on the flat ends of the cylinder, to illuminate the inner surface of the curved walls, symmetrically about the cylinder axis. [22]. The hohlraum walls are typically made of some combination of high-Z materials, such as gold and uranium. These materials have a high opacity to the thermal radiation field present in the hohlraum, and this keeps radiative heat losses to a minimum [23]. The temperature of the hohlraum can be determined by a power balance analysis involving the incoming laser power, and the radiative heat losses to the wall, laser entrance holes and capsule surface [24]. A fraction of the X-rays generated at the wall heat up the surface of the fuel capsule resulting in its implosion, ignition and burn as previously described [21]

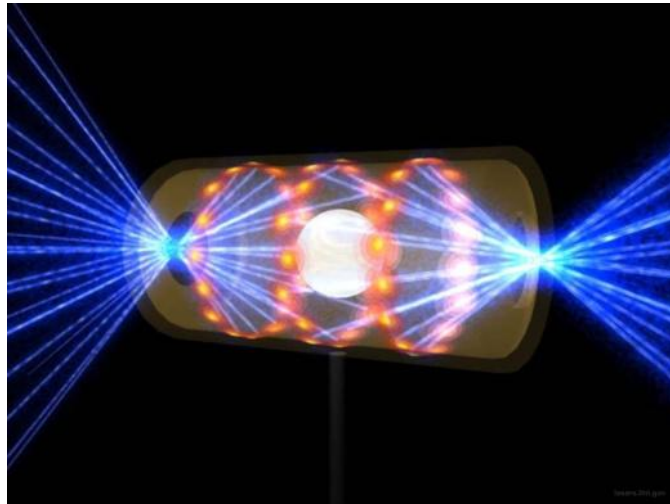


Figure 1.7. Shows a NIF target pellet inside a hohlraum capsule, laser beams entering through the openings on both sides of the hohlraum cavity and heat the walls of the cavity. Radiations are emitted from the walls in the range of soft X-rays (hohlraum acts as a black body). The radiation beams emitted from the walls of the cavity compress and heat the target to acquire the necessary conditions for ignition [22].

Conversion of laser light into x rays has the advantage of removing the capsule surface from any spatial non-uniformities present in the laser beam, or which would be present as a result of overlapping the beams at the capsule surface. However the laser spots must be carefully placed on the hohlraum wall, and the hohlraum wall sufficiently far away from the capsule, that the radiation field experienced by the capsule is not unduly perturbed by the laser hotspots on the hohlraum wall. These laser interaction regions are out of radiative equilibrium with the rest of the hohlraum. By removing the laser interaction regions from the capsule surface, indirect drive can potentially be more robust against the RTI than direct drive, however a substantial fraction of beam energy is lost in this

process. Most of the energy of the driver actually goes into heating the hohlraum walls, rather than imploding the capsule [25].

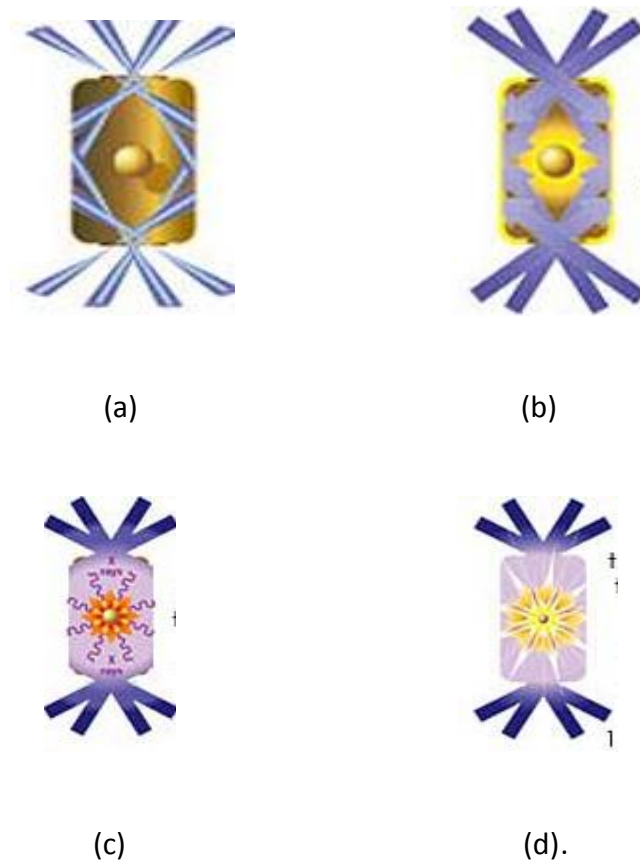


Figure 1.8. Indirect drive sequence a) Laser beams rapidly heats up the inner walls of the cavity. b) X-rays from the walls of the hohlraum irradiate the surface of the capsule fixed at the centre of hohlraum and implode the fuel. c) The core of the fuel target ignites, a burn wave propagates outwards from the centre of the target . d) Burn spreads through the compressed fuel [17], [22].

This scheme is not very practical from an energy production standpoint because of this inherent inefficiency and also because of the complexity and cost of the integrated hohlraum/fuel capsule targets [17].

1.5.2 Direct drive implosion

In a direct drive inertial confinement fusion implosion, fuel capsule is directly heated by the intense energetic beams (either laser beams, ions or electrons), usually a very large number of high intensity pulsed laser beams of equal intensities are focused onto the target surface, resulting in a symmetrical ablation pressure at the fuel capsule surface[11], [17], [20].

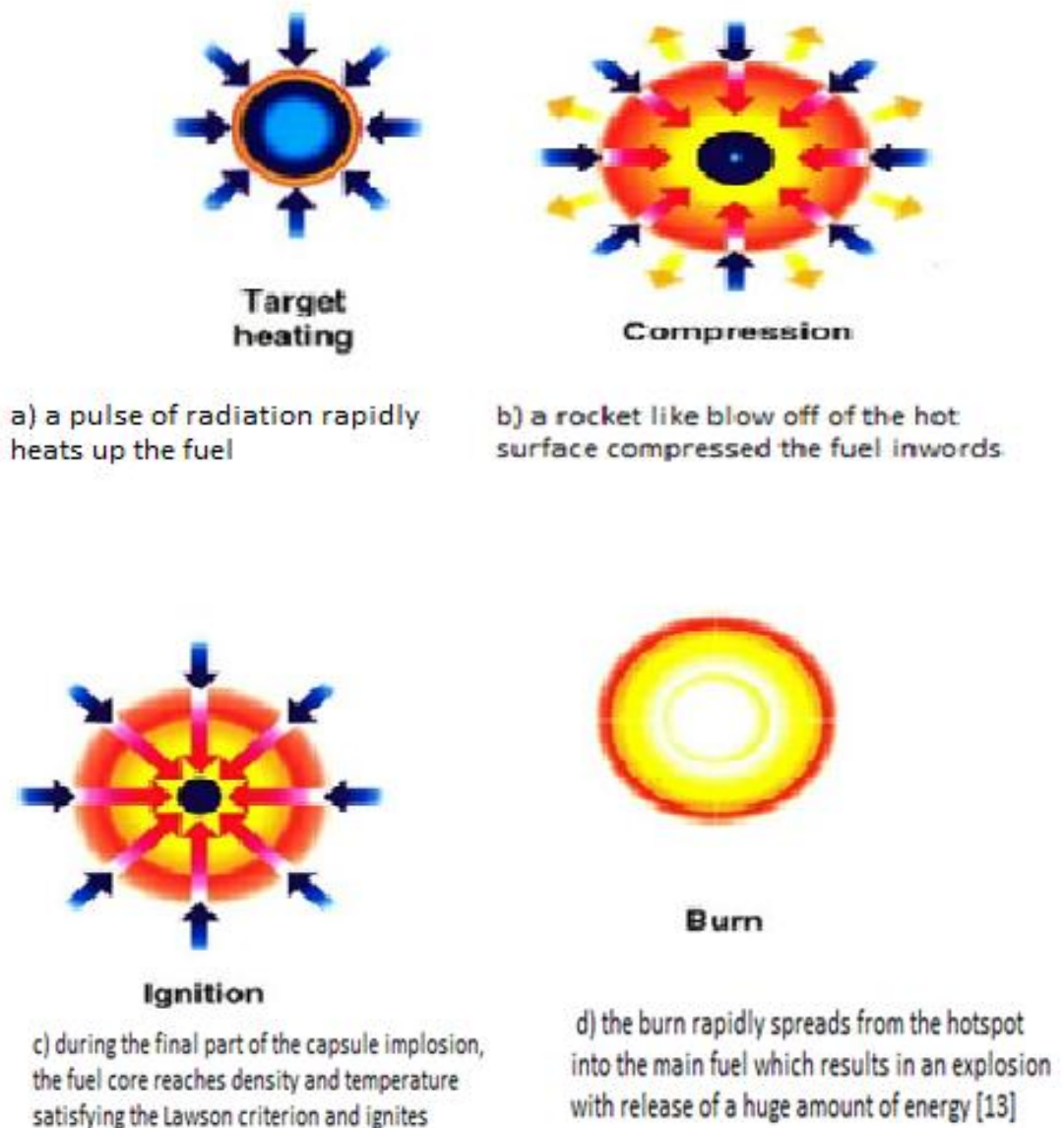


Figure 1.9. Central hot spot inertial confinement fusion [26].

The main advantages of direct drive are clear from the preceding section on indirect drive. It is efficient; and it uses a simple and therefore relatively inexpensive target. The downside of this, compared to indirect drive, is that such targets are far more susceptible to laser non-uniformities driving the RTI.

1.6 Central hotspot vs. Fast Ignition

So far we have only discussed approaches to ICF which proceed by so called “central hotspot ignition” [11], [20]. As previously mentioned, at stagnation, the pressure is balanced between main fuel and hot spot, therefore such schemes are sometimes labelled “isobaric” [20].

Central hotspot ignition requires energy in the Mega-Joule range to start the ignition process; the reason for this is that the efficiency of the fuel heating is very low (~1%). In addition this approach is challenging since it requires that substantial attention be paid to avoiding the RTI [11].

This inherent inefficiency and the very demanding symmetry requirements make the central hotspot ignition process a poor candidate for energy production [19].

In 1994 another scheme was proposed. In this scheme the compression and heating phases are separated [6], and ignition occurs in non-isobaric fuel. Such schemes are termed “fast ignition” schemes. Fast ignition concepts aim to both improve fuel heating efficiency, and also to reduce susceptibility to the RTI. It is this fast ignition approach, which will be described in more detail in the next chapter, that provides the basis for the research described in the remainder of this thesis.

1.7 References

- [1] S.E. Hunt, Fission Fusion and Energy Crisis, 2nd Edition, Pergamon Press, [1980].
- [2] E.W. Brown , An Introduction to Solar Energy, [1988].
- [3] Canada's Energy Future , National Energy Board [2006].
- [4] www.gohybrid.ca/alternative_energy.html.
- [5] www.thesocialcontract.com/artman2/publish/tsc1602/article_162.shtml
- [6] www.pbl.nl/en/publications/2009/Global-CO2-emissions-annual-increase-halves-in-2008.
- [7] R. Swarup, Fossil Fuel and The Environment, 1st Edition, Mittal Publications, [1992].
- [8] A. Devolpi et al., Nuclear Shadow Boxing, Legacies and Challenges , **2**, [2005].
- [9] http://ec.europa.eu/research/energy/euratom/fusion/atglance/history/index_en.htm.
- [10] K.S. Krane, Introductory Nuclear Physics, 1st Edition, John Wiley and Sons Ltd, [1988].

-
- [11] S. Atzeni and J. Meyer-Ter-Vehn, *The Physics of Inertial Fusion*, Oxford Science Publications, [2004].
- [12] P.C. Souers, *Hydrogen Properties for Fusion Energy*, The University of California Press, [1986].
- [13] P.A. Tipler and R.A. Llewellyn, *Modern Physics*, 4th Edition, W.H. Freeman and co, [2002].
- [14] Nuckolls et al., *Nature*, **239**, 129, [1972].
- [15] J.D. Lawson, *Proceedings of the Physical Society*, **70**, 6, [1957].
- [16] S. Nakai and H. Takabe, *Reports on progress in physics*, **59**, 9, [1999].
- [17] R.J. Hawryluk et al., *Physics of Plasmas*, **5**, 1577, [1998].
- [18] www.hiper-laser-org.
- [19] J.D. Lindl, *Inertial Confinement Fusion*, AIP Press, Springer-Verlag, [1998].
- [20] S. Atzeni et al., *Plasma Physics and Controlled Fusion*, **51**, 015016, [2009].
- [21] J.D. Lindl, *Physics of Plasmas*, **2**, 3933, [1995].
- [22] <http://quantprinciple.com/qboiler/icf.html>.
- [23] OS. Jones et al., *Physics of Plasmas*, **14**, 056311, [2007].
- [24] J.D. Kilkenny et al., *Hohlraums Energy Balance*, Lawrence Livermore National Laboratory, [1994].

[25] S. Atzeni et al., *Plasma Physics and Controlled Fusion*, **46**, B111, [2004].

²⁶[26]<http://www.anthonares.net/2006/02/imploding-pellets-fusion-and-the-worlds-biggest-laser.html>.

The Role of the Author

The role of the author was to analyse the electron spectroscopy data taken in the experiment that is outlined in Chapter 3 of this thesis, in order to produce the results and analysis that is to be found in Chapter 4. The experiment itself was performed by the author's colleagues from the University of York, as well as collaborators from the Rutherford Appleton Laboratory and the University of California San Diego. The experiment was further supported by expertise and resources from St Andrews University, the Lawrence Livermore National Laboratory and General Atomics. The experiment was designed by my supervisor, Dr John Pasley, and the related K- α analysis has been performed by my fellow student at the University of York, Mr Ian Bush.

At the time of writing a publication resulting from the experiment outlined in Chapter 3 has been drafted and circulated amongst co-authors in preparation for submission to Physical Review Letters:

Effect of Defocusing on Picosecond Laser-Coupling into Gold Cones, I. Bush, L. Gartside, S. Sarfraz, E. Wagenaars, J. Green, M. Notley, H. Lowe, C. Spindloe, T. Winstone, A. P. L. Robinson, R. Clarke, T. Ma, T. Yabuuchi, M. Wei, F. N. Beg, R. B. Stephens, A. MacPhee, A. J. MacKinnon, M. H. Key, W. Nazarov, and J. Pasley, being prepared for submission to Phys. Rev. Lett., [2011]

Chapter 2

2.0 Fast Ignition

As we have discussed in the first chapter, for conventional ICF the target should be highly symmetrical, it also requires high ablation pressure symmetry. On the basis of this scheme scientists in Japan and USA were able to perform experiments in the 1980's using the Gekko XII laser that achieved a fuel compression of about 600g/cc [1]. However, they were unable to assemble sufficient fuel, or raise it to a sufficient temperature, that the ignition criteria, discussed in Chapter 1, could be met. The target symmetry and the ignition energy requirements make it difficult to achieve ignition using the conventional central hot spot approach [1].

These difficulties have made the scientists consider many routes to improving the basic central hotspot ignited ICF target design, and have also focussed efforts upon other areas, such as the improvement of laser beam quality. As

with the original idea of ICF, it was a development in technology that suggested a key breakthrough. This technological achievement was the development of petawatt lasers. The development of these ultra-short pulse petawatt lasers opened up new possibilities to those interested in laser driven fusion research' [2].

In 1994 Tabak et al proposed an idea that was quite distinct from the conventional central hot spot approach to ICF. This scheme separates fuel compression from fuel heating. They named it fast ignition. Fast ignition is an attractive scheme which relaxes not only the symmetry requirements of the target capsule implosion, it also promises to relax overall driver energy requirements [3].

The fast ignition scheme potentially reduces the required energy for ignition by aiming to produce a hotspot in a manner that is substantially more efficient than the compressive approach employed in the central hot spot scheme. Furthermore, it aims to achieve ignition in fuel that has been assembled to lower densities. If we look at the figure 2-1 [4], [5] then we can see that in the case of fast ignition, the density and ablation pressure requirements are low as compared to the conventional hot spot ignition. It is also apparent that whilst, at the end of the implosion, the conventional ICF target has two distinct regions of temperature, this is not the case with the fast ignition target (at least ideally). In fast ignition, the ignition driver requirement is low for two reasons: firstly this scheme aims to ignite by a mechanism that is more efficient than compressive

heating; secondly it aims to ignite in denser fuel, which results in a smaller hotspot mass, as compared to the conventional central hot spot scheme, as we can see from figure 2.1. We can understand this by a simple relationship. We know that for ignition the hotspot must have $\rho r > 0.3\text{g/cm}^2$ [5]. If the hotspot is roughly spherical (a not unreasonable approximation), then this implies that a high density hotspot can reach the ignition with a substantially lower mass, since, $M = \frac{4}{3} \rho \pi r^3$. This further implies that the energy required to heat that mass is much reduced.

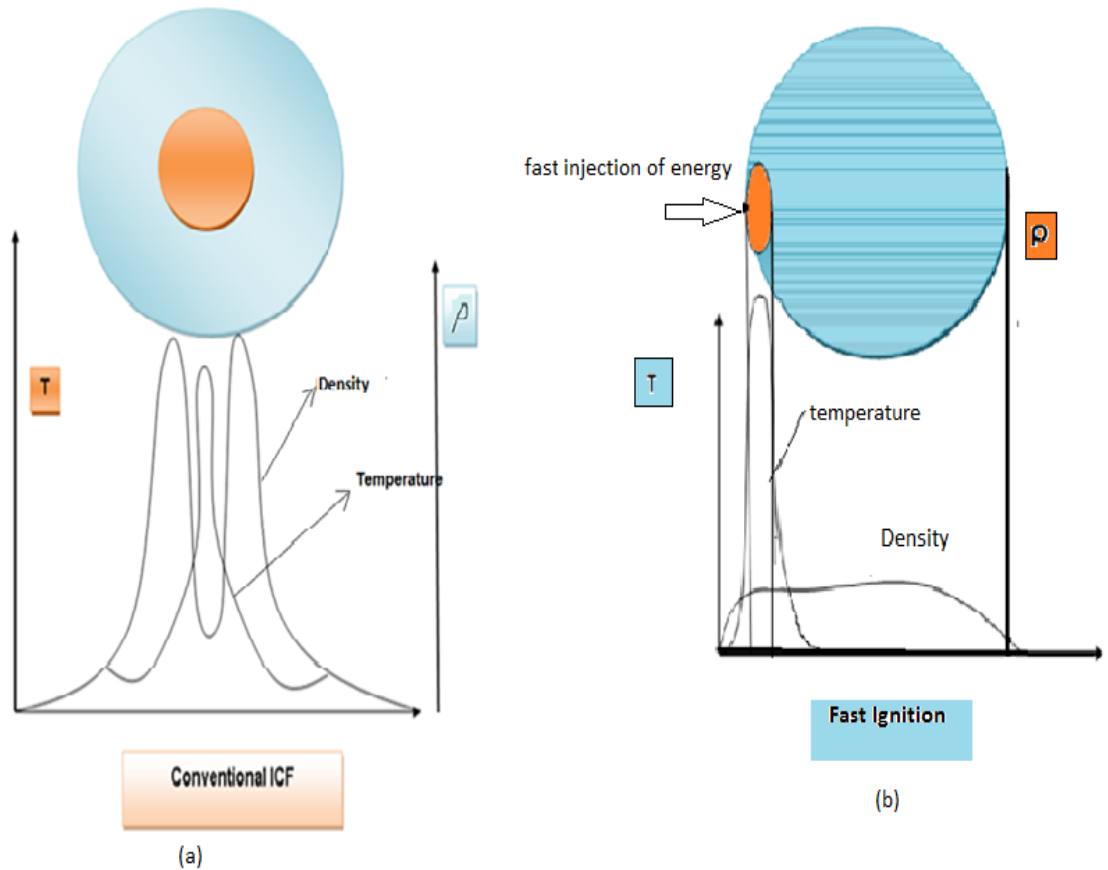


Figure 2.1. The difference between the two schemes for hot spot generation and the achievement of ignition is shown schematically with (a) representing conventional hot spot ignition and (b) showing fast ignition [6]. In the conventional hot spot ignition case, a hot spot is formed at the centre of the DT capsule by the converging shell. This results in isobaric conditions. In the case of the fast ignition, all of the fuel is compressed to a similar density, and a fraction of the DT is heated by an external source (the ultra-intense laser) to form the hot spot. This hotspot is then out of pressure equilibrium with the surrounding fuel [9].

The characteristic trajectories of the thermodynamic quantities in the hot spot and in main fuel are shown in Figure 2.2. Isobaric and isochoric compression model are respectively used to describe the behaviour of the fuel during the ignition [25].

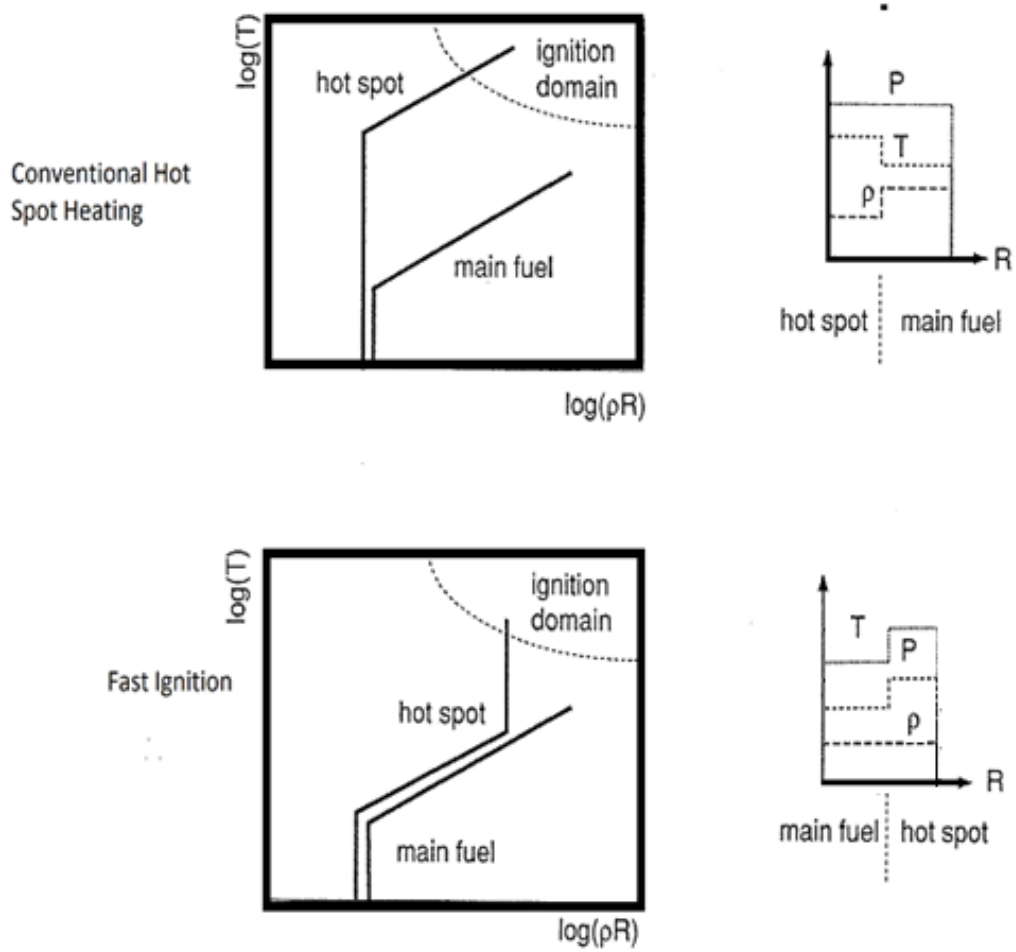


Figure 2.2. Isobaric and isochoric compression model are respectively used to describe the behaviour of the fuel during the ignition in conventional central hotspot ignition and fast ignition [25].

Fast ignition requires an ultra-short petawatt laser pulse to heat a region near the surface of the dense fuel blob to ignition conditions, and so start a burn wave propagating across the imploded fuel [2]. The spatial scale of the hotspot, and the time available for the heating dictates that the focussed laser intensity must be upward of 10^{20} W/cm². There are two basic schemes for fast ignition, the hole-boring and the cone-guided schemes. Both of these schemes aim to circumvent the major barrier to fast ignition, which is that the igniter laser can only propagate to the point where the laser frequency equals the electron plasma frequency. This density is usually thousands of times lower than the density of the compressed fuel, where the laser must deposit its energy [6]. This so called critical density surface is also usually separated from this dense region by a substantial distance (hundreds of microns).

2.1 Hole-boring scheme or self-focusing scheme

This is the scheme which was originally proposed by Tabak et al, and it is based upon boring a hole through the under dense plasma that surrounds the dense fuel core using the light pressure of an intense laser pulse. This scheme can be most easily explained if we divide it into three phases [7], [8], [9].

-
- 1) Compression
 - 2) Hole boring
 - 3) Ignition

The first phase is the same compression phase as occurs in the conventional central hotspot ICF, however shock strengths and implosion velocities are limited such that the central hotspot is rather cold by comparison, and the imploded densities are also limited. In the second phase of the hole boring scheme, a short pulse laser beam (usually ~ 100 ps in duration) 'drills' a hole through the under dense plasma surrounding the dense fuel core. This hole acts as an open channel which is relatively free of plasma for the ignition pulse to reach the pre-compressed fuel with minimum energy loss. In the third phase an ultra-short pulse with a power in excess of a petawatt is used to ignite the fuel [7]. The ignition pulse interacts with the under-dense plasma near the dense region at the far end of the channel that has been bored by the preceding hole-boring pulse. Relativistic electrons are generated during this interaction and are ejected from the region at the end of the channel. A significant fraction of these electrons then deposit their energy into the dense fuel, creating a hotspot and triggering the ignition of the imploded fuel mass. The igniter pulse is timed to coincide with the achievement of maximum fuel ρR , to an accuracy of a few 10s of ps. It is estimated that ignition of fuel is possible if approximately 10kJ of energy is delivered to a compact hot spot at the edge of the dense fuel mass in 10ps [10]. This time period is set by the disassembly time of the hot spot [11].

A number of issues relating to the hole-boring scheme remain to be resolved. It is difficult to control the hole-boring laser pulse while it is passing through the coronal plasma [12]. It has been observed that in many cases the laser light has a tendency to break up into a number of filaments and be scattered away from the dense fuel [3], [11]. In terms of the scheme as a whole, significant work still needs to be done to understand how to generate a path through the corona which remains free of plasma for sufficient time that the igniter energy can reach the core without excessive energy loss [13]

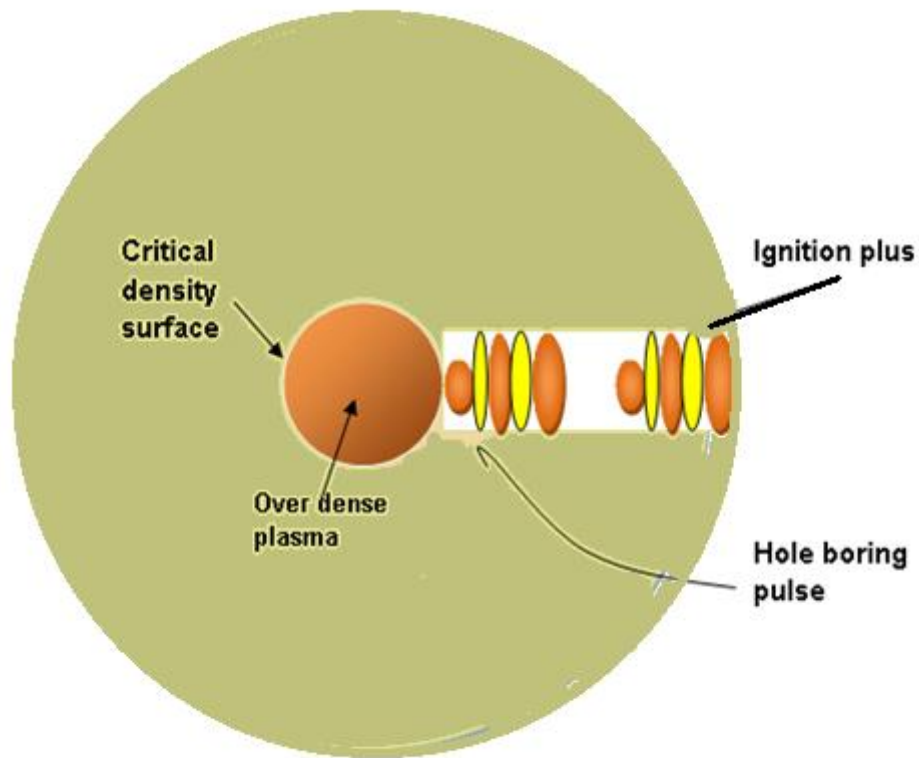


Figure 2.3. Laser hole boring scheme [14].

The hole boring scheme is based on three stages, 1st the fuel is compressed in same way as in conventional hot spot ICF. A short-pulse laser beam delivers energy just prior to the time of maximum compression to bore a channel ($n < n_c$) through the ablated part of the capsule (hole boring phase). A second shorter laser pulse (PW laser pulse) aligned with the boring laser propagates into the channel created by the 1st laser, to the hot core of the fuel. This fast transfer of laser energy to the compressed fuel occurs via very energetic electrons which are created when the laser interacts with the corona surrounding the hot core, called suprathermal or fast electrons. These electrons propagate to the core of

the pre-compressed capsule and deposit their energy. This rapid heating increases the temperatures of hot spot in the fuel and ignition starts [9].

These issues are very important to resolve for a successful hole-boring scheme. Scientists are still struggling to resolve these problems.

A few years after Tabak et al's original proposal, researchers developed another scheme in which a high-Z cone is imbedded into the surface of the fuel capsule, providing a plasma free path to the dense core. This scheme of fast ignition is referred to as the cone-guided fast ignition scheme [15].

2.2 Cone-guided fast ignition

The cone-guided fast ignition scheme uses a hollow cone to provide a path for the ignition laser pulse to reach the dense fuel without having to interact with the under-dense coronal plasma. The capsule is imploded to form a dense fuel blob sitting just forward of the tip of the cone as shown in the figure [15], [16], [17]. The ignition laser beam is then focused onto the interior of the cone tip. The relativistic electrons then need only traverse the cone tip and the relatively short distance of dense plasma between the cone tip and the densest regions of fuel [13], [18].

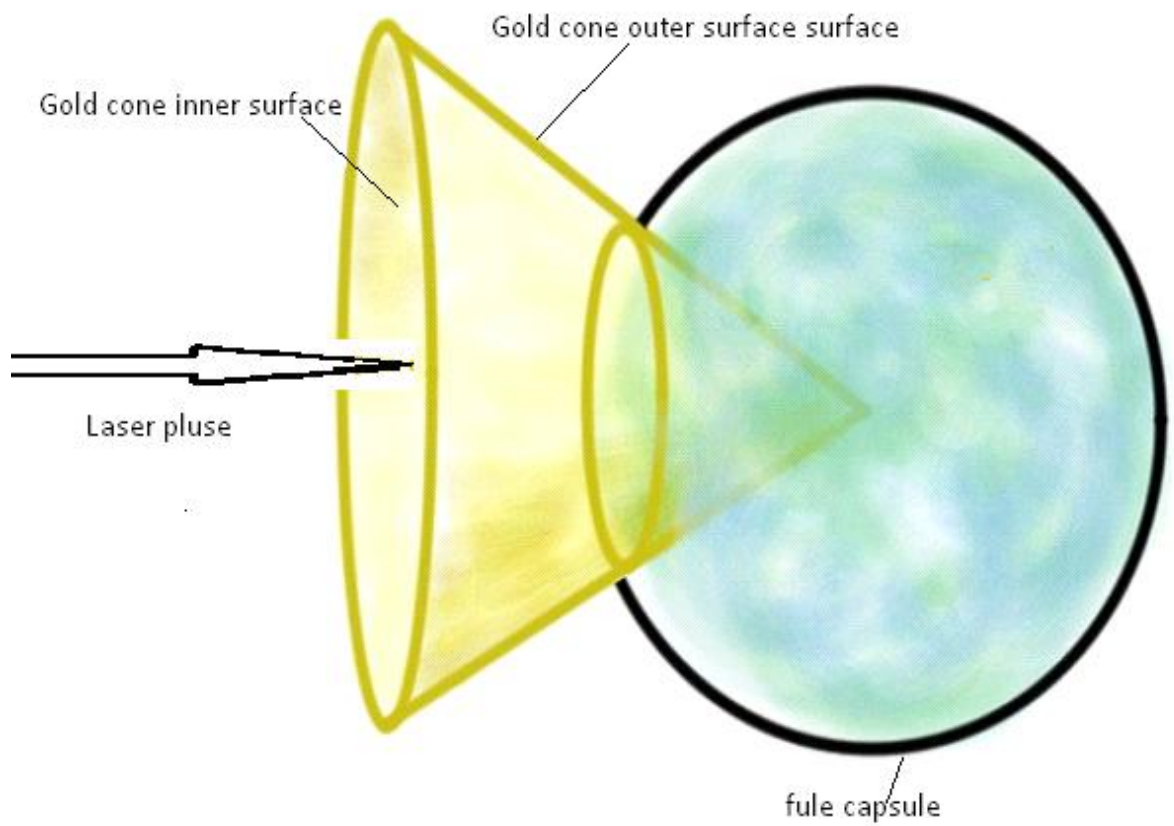


Figure 2.4. Cone guided target [19].the target consist of a hollow gold cone with a closed tip, embedded into the side of a DT filled spherical fuel capsule.

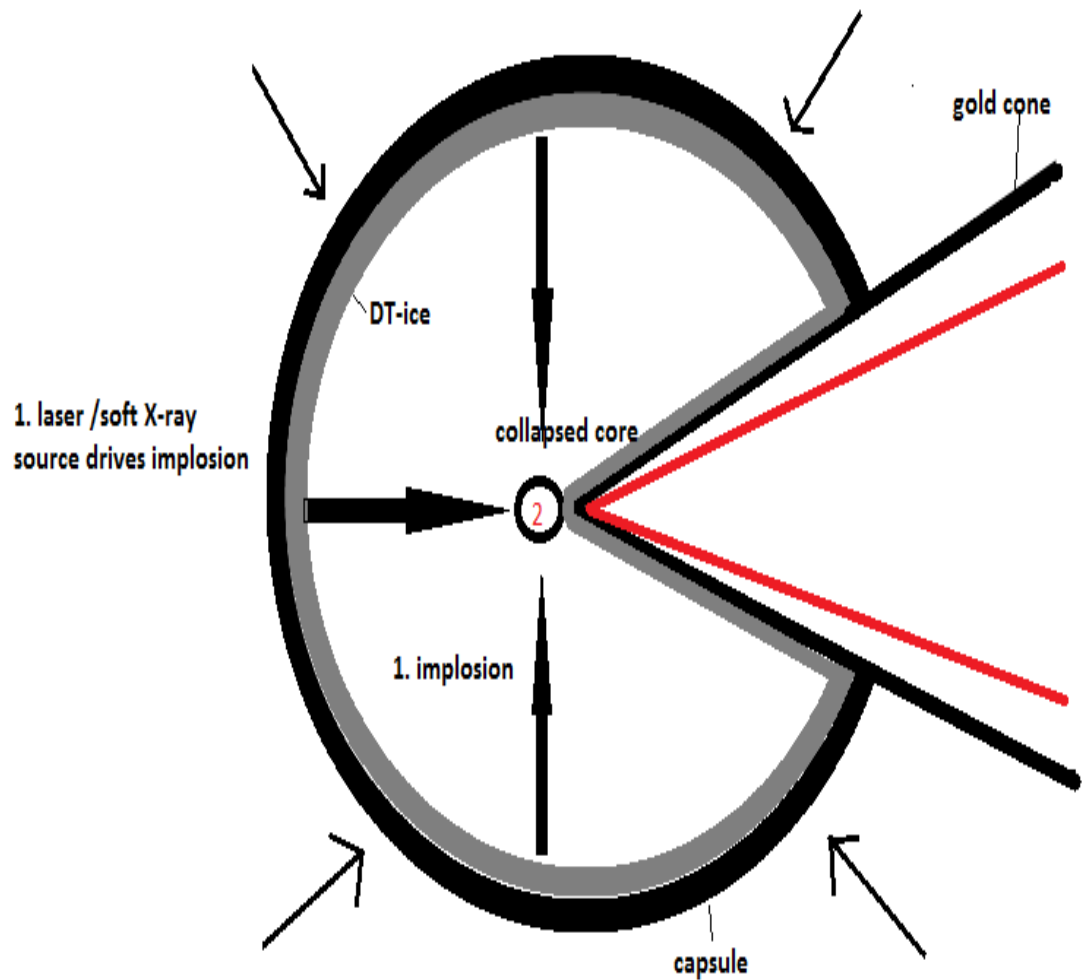


Figure 2.5. When the laser pulse interacts with the walls of the cone, plasma is created inside the cone and fast electrons are generated. The electrons generated inside the cone have to travel only a few tens of micrometres from the cone tip to reach the compressed fuel, igniting it at the time of stagnation [20].

Fast electrons generated inside the cone have a tendency to be conducted along the walls of the cone. Some hope that the conical geometry, combined with the

influence of self-generated electrical and magnetic fields can enhance the fast electron density at the tip of the cone [17]. Although some experimental results raise question marks about the guiding effect of the cone, this is an area that is still poorly understood [21].

2.3 Hot electron generation and transportation in short pulse laser- solid target interaction

A knowledge of the mechanisms of hot electron generation and transportation in short pulse laser-plasma interactions is very important if we are to understand the complete physics of fast ignition. In fast ignition it is these electrons which transport energy to the pre-compressed core and trigger ignition [22]. Scientists are still struggling hard to understand the mechanisms of electron generation and transportation in short-pulse laser-plasma interactions with solid targets; the facts remain ambiguous [3].

When the igniter pulse interacts with the background plasma energetic electrons are generated due to several different heating mechanisms. As these electrons move further into the bulk target, strong electric and magnetic fields are generated due to the motion of the electrons which in turn affect those electrons which are entering the target. Self-generated electric and magnetic fields can act both collimate the electrons and also to prevent them from entering the target [23].

The Laser beam intensity is the key parameter in determining which mechanisms of electron generation and transportation will occur in the target. At the intensities relevant to fast ignition, the dominant mechanism is ponderomotive acceleration. Electrons acquire MeV energies and move with the velocities approximately equal to the speed of light. The energetic electrons propagate into the dense plasma. Ideally, the majority of these hot electrons will be stopped in the dense plasma within the necessary ρR to form a compact hotspot. These fast forward moving electrons are compensated either by the cold return current or by refluxing of the energetic electrons. The generation and transportation of electrons is effected by a range of factors including [2]:

- 1) Laser beam intensity.
- 2) Laser beam incidence angle.
- 3) Polarization.
- 4) Plasma scale length.
- 5) Target material.

As, in the experiments discussed later, we are dealing with such high power short pulse laser beams interacting with solid targets, it is appropriate to discuss some of the relevant phenomena.

2.4 Ponderomotive acceleration

In case of laser intensities of relevance to fast ignition, electrons are accelerated under the action of laser ponderomotive pressure [3]. The laser electric field exerts a force perpendicular to the direction of laser incidence [19]. The magnetic field, on the other hand, exerts a force in the laser incidence direction [20]. The magnitude of the force of the magnetic field is equal to that of the electric field when $v/c \sim 1$ [3]. The combined effect of these forces produces a longitudinal component to the ponderomotive force which acts to accelerate electrons along the laser propagation path [2]. This forward going component to the electron acceleration is critical for fast ignition since it results in electrons being accelerated toward the dense fuel core.

2.5 Ohmic inhibition and heating

When laser light hits the target the energy is transferred from laser light to relativistic electrons. As these electrons penetrate into the target, they generate a charge imbalance and consequent electric field. The energetic electrons have a long mean-free-path, and so are not directly affected by the resistivity of the background fluid. However the electric field draws a return current of electrons from the background plasma. These electrons have a temperature characteristic of the plasma background (few hundred eV to few keV) and therefore are affected by the resistivity of the fluid. This results in Ohmic heating of the fluid.

However the self-generated E-field of the relativistic forward going electrons can reach such a magnitude that it inhibits the forward flow of energy into the target. Over longer time scales self-generated magnetic fields can also grow to the point of inhibiting energy flow [24].

2.6 References

- [1] S. Nakai and K. Mima, *Reports on Progress in Physics*, **67**, 321–349. [2004].
- [2] S. Atzeni and J. Meyer-Ter-Vehn, *The Physics of Inertial Fusion*, Oxford Science Publications, [2004].
- [3] O. Willi, *The Royal Society*, **357**, 555-574, [1999].
- [4] www.lasers.llnl.gov/fast_ignition.php.
- [5] L.J. Perkins, Lawrence Livermore National Laboratory, UCRL-ID-TR-20085, [2003].
- [6] J. Pasley, *Pramana*, **75**, 759-767, [2010].
- [7] H. Takabe *et al.*, *Plasma Physics and Controlled Fusion*, **41**, 3A, [1999].
- [8] M.H. Key, *Nature*, **412**, 775-776, [2001].
- [9] C. Deutsch, *Eur. Phys. J. Appl. Phys*, **24**, 95–113, [2003].
- [10] A. Pukhov and J. Meyer-ter-Vehn, *Physical Review Letters*, **79**, 14, [1997].
- [11] V.T Tikhonchuk *et al.*, *Journal of Physics: Conference Series*, **244**, 022069, [2010].
- [12] Y. Sentoku *et al.*, *Physics of Plasmas*, **11**, 3038, [2004].

-
- [13] P.A. Norreys et al., *Physics of Plasmas*, **7**, 3721, [2000].
- [14] fsc.lle.rochester.edu/meetings/livermore2010/RefFSC2010.ppt.
- [15] <http://www.hiper-laser.org/docs/tdr/hipertdr.pdf>.
- [16] J. Meyer-ter-Vehn et al., *Plasma Physics and Controlled Fusion*, **43**, 12A,[2001].
- [17] A.L. Lei et al., *Physics Review Letters*, **96**, 255006, [2006].
- [18] S.D. Baton et al., *Physics of Plasmas*, **15**, 042706, [2008].
- [19] www.stanford.edu/~rhamerly/cgi-bin/Ph240/Ph240-2.php.
- [20] www.york.ac.uk/physics/research/plasmaphysics/research/laser/laserfi/.
- [21] J.J. Honrubia et al., *IOP Publishing*, **51**, 014008, [2009].
- [22] L.M. Chen et al., *Physics of Plasmas*, **8**, 6, [2001].
- [23] L.M. Chen et al., *Physical Review Letters*, **87**, 22, [2001].
- [24] A.R. Bell et al., *Physical Review Letters*, **59**, 6032–6036, [1999].
- [25] J. Meyer-ter-Vehn, *Nucl. Fusion* **22**, 531 ,[1982].

Chapter 3

3.0 Electron Spectroscopy

A range of diagnostic techniques have been used so to investigate the phenomena of electron generation and transport relevant to the fast ignition scheme for ICF. The most important component of the fast ignition process is the transfer of energy from the intense laser to the fuel. In case of the fast ignition, the fast forward moving electrons transport energy to heat a portion of the compressed fuel core to high temperatures. Although a number of different types of targets and diagnostics have been employed to date to investigate the phenomena of energy transfer, a number of issue still remain unclear [1].

Low mass targets are interesting as they can be tackled in their entirety by detailed numerical modelling [2]. The foil targets can be used to show the divergence of the energy transport which leads to poor coupling to the core in a

FI experiment. The divergence of the electrons is hard to model as the divergence of the fast electron emitting from the target is critically influenced by the characteristics of the electron source [2]. Thin foil targets require a very high contrast ratio between laser main pulses and pre-pulse, approximately $<10^{10}$. Otherwise a high intensity pre-pulse could launch a shock wave that can destroy the target before the main pulse of the laser arrives [3] also significant pre pulse can generate pre-plasma at the target front surface which can substantially affect the electron generation and transport [4] Experimentally, this effect can be reduced by using a plasma mirror which can control the pre-pulse [3]. It has been seen in many experiments that the emitted electron beam radius rapidly becomes much greater than the incident laser focal spot. This shows that the electrons are emitted with a large divergence angle [5]. If the divergence angle is too large then the required laser pulse energy is very high to ignite the fast ignition fuel [6].

A cone wire target with a thin wire is also a relatively simple geometry for numerical modelling, although the total mass of the target including the cone is too great to enable comprehensive PIC modelling to be employed [2]. A number of experiments have been employed to date so far employing cone attached wire targets to investigate the generation and transportation mechanisms of fast electrons in high energy laser solid interaction. it is not possible to discuss all of them but we will briefly discuss a few experiments in which cone wire targets were employed to investigate the electron transport.

If we have a look on the cone wire experiment done by J.A. King et al the analysis shows that the hot electrons have a Maxwell–Boltzmann distribution function [7]. These hot electrons are ejected into the axial length of the wire attached to the cone. Results shows that the hot electron current must be compensated by cold return current, this cold current contributes to heat the wire by Ohmic heating [8]; at the same times it creates a potential which strongly resists the axial penetration of hot forward electron current [9].

The experiment discussed in this thesis was performed in November-December 2008 at the Rutherford Appleton Laboratory using Vulcan Petawatt Laser. Vulcan is a neodymium doped glass laser. The Petawatt arm of the Vulcan system is a chirped-pulse amplified beam line capable of delivering ~ 600 J in ~ 1 ps , focused using a f/3 parabolic mirror to an $8\mu\text{m}$ (FWHM) spot to achieve peak intensity on the order of $\sim 10^{21}$ W/cm² [10].

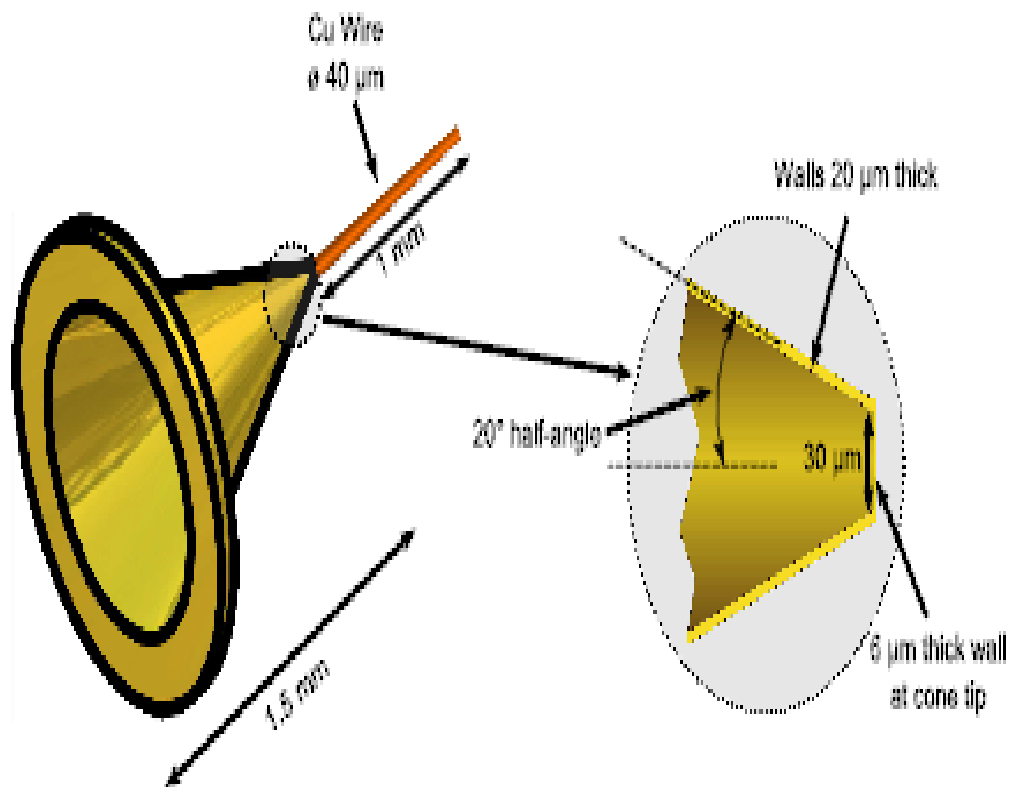


Figure 3.1. Figure explains the dimensions of the gold cone and the wire attached to the cone.

Gold cone-wire targets, as illustrated in figure 3.1, were used in the experiment. The length of the cone walls are 1.5mm with a thickness of 20μm and a 20⁰ half angle. Forty micron diameter copper wires of different lengths were attached to each cone to investigate the transport of fast electrons forward of the cone tip.

The chamber setup for the following experiment is shown in the figure 3.2.

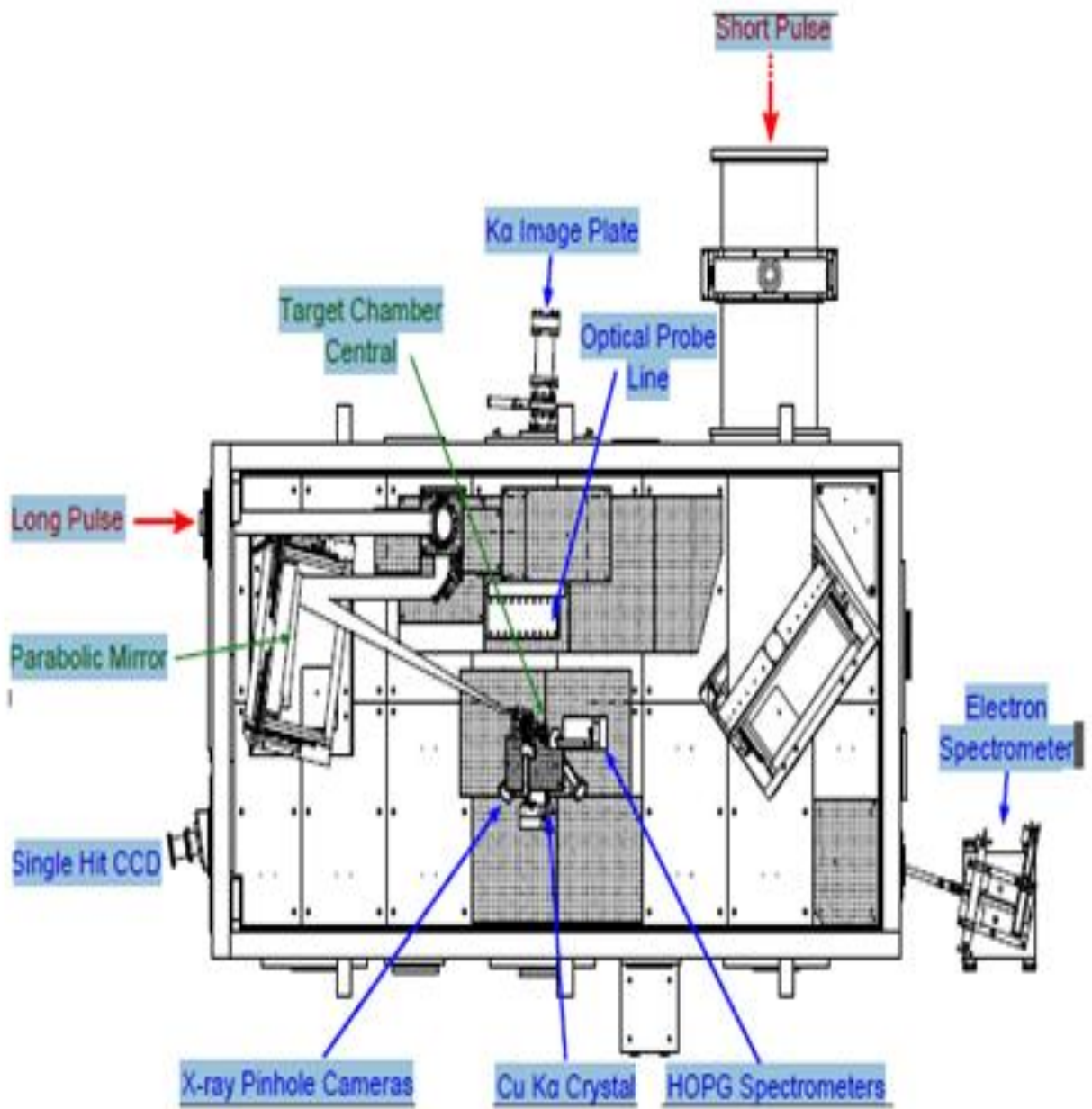


Figure 3.2. The chamber setup shows different diagnostics are fielded.

Figure 3.2 shows that Cu-K α crystal diagnostics were set up, as well as a 2D crystal imager, a pair of HOPG (highly oriented pyrolytic graphite) spectrometers and a single photon counting CCD camera. The other primary diagnostic used were an optical probe and an electron spectrometer. A pair of X-ray pinhole cameras were also fielded. The analysis performed by the author that is presented in detail in this thesis is based entirely upon the data collected by the electron spectrometers. The nature of some of the other diagnostics fielded, and their purpose, is mentioned briefly below.

3.1 K- α diagnostics

3.1.1 HOPG Spectrometer

A pair of highly oriented pyrolytic graphite (HOPG) spectrometers with Fuji Film image plate (IP) detectors are fielded to record the variations in K- α spectra as the focus position of the laser is changed. The HOPG spectrometer is placed such that it views the emission from the front of the target. The image plate is covered with 5 μ m of aluminium foil to avoid direct exposure of visible light to image plate. The whole assembly is placed inside a lead housing to reduce the background noise due to the x-rays scattered from the walls of the target chamber [11].

3.1.2 Cu K- α crystal imager

A spherically bent Bragg crystal is employed to image the K- α emission from the wire onto an IP. This diagnostic gives information about the hot electron spectrum present inside the solid target, by examining the manner in which the intensity of the emission varies with depth (distance along the wire) [12], [13].

3.2 Single Hit CCD

An absolutely calibrated single hit CCD was used to measure the absolute K- α yield on each shot. The camera used was a Princeton Instruments SX1300 camera, with a pixel size of 20 μ m \times 20 μ m and a total area of 1300 \times 1340 pixels [14]. The role of this diagnostic is principally as a calibration device for the HOPG spectrometers and K- α crystal imager, permitting the signal strength from each to be related to an absolute intensity of K- α emission.

3.3 Electron spectrometer

The electron spectrometer is aligned such that it looks straight down the axis of the cone wire from the target rear surface. A collimator is fixed at the entrance

of the spectrometer [14] which blocks electrons from entering the spectrometer other than from the direction of the target [15]. When these electrons enter into the magnetic field inside the spectrometer body, they disperse according to their energies and hit a strip of image plate [16]. The spectrometer is carefully designed to provide a cylindrical volume of uniform field strength [15]. Electrons then follow the Larmor motion as determined by their kinetic energy. Electron with different energies will then strike the image plate at different locations providing a spectrally dispersed record of their intensity [15].

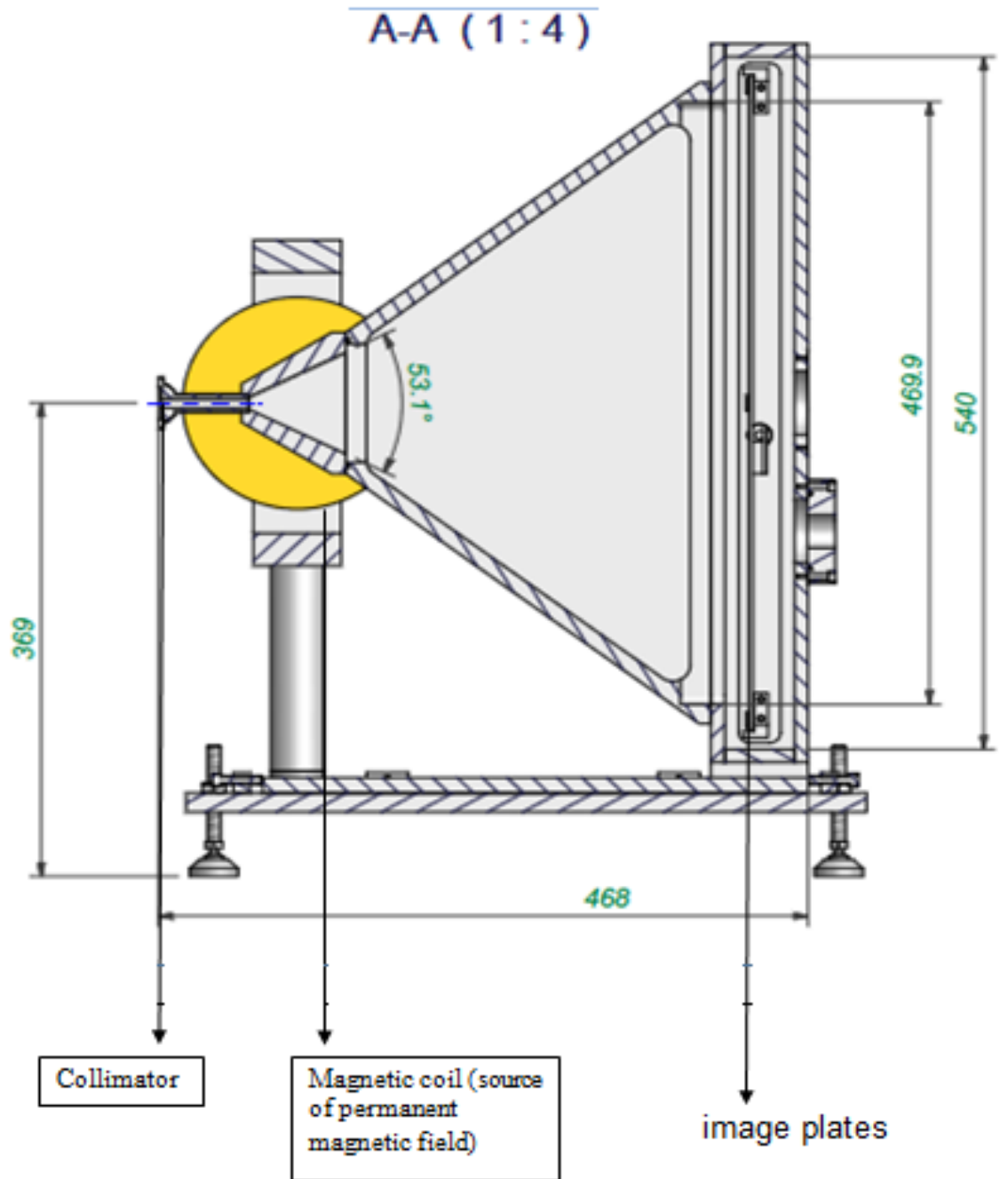


Figure 3.3. Electron spectrometer. Shows entrance (collimator), magnetic coil and image plate.

3.4 Image Plates (IP)

Image Plate (IP) consists of a phosphor image sensor which is designed to replace X-ray film [17]. IP has wide applications in X-ray detection and imaging due to its properties: wide dynamic range ($\sim 10^5$), high detective quantum efficiency (DQE) and better linearity and sensitivity compared with photographic film. It has high sensitivity (defined as PSL intensity per electron) [18]. IP is not affected by the electromagnetic pulse noise while the detectors with electrical circuits could be affected by the strong electromagnetic pulse [1]. Image Plates separate two basic operations: recording the radiation dose and reading the data. The sensitive electronics are confined to the reader, which can be located remotely away from the experiment, where it will not be at risk [19],[20].

IP is composed of a protective layer, a photo stimulated phosphor layer and a support. [20]. The thickness of protective plastic layer can vary from 0 to 10 μm according to application because the thickness affects the intensity of radiation reaching the active areas. Naked Image Plate is used for low intensity radiation [21]. The effective component of IP is a photo-stimulable phosphor layer. The thickness of this layer can be varied between 50—180 μm [21] and is composed of cubical ion crystal BaFX:Eu^{2+} ($X = \text{Cl, Br or I, typically } X = \text{Br}_{0.85}\text{I}_{0.5}$) [19]. The support of an Image Plate also varies according to the needs of an experimental setup. IP records the electron radiation because of its photo-stimulatable layer [21].

The raw data collected on an image plate is QL data, a converter is used to convert this data into PSL level. The PSL level is calculated as (according to the formula given by Fuji Film Corporation) [19], [22] :

$$\text{PSL} = (\text{pix}/100)^2 \times 4000/\text{s} \times 10^{L(\text{QL}/G - 0.5)}$$

Where, pix is size of pixel (in um), S is the sensitivity, and L is the exposure range, QL is the gray scale value of the pixel of interest, and G is the depth of the scan [22].

Once the data is stored on Image Plates one should consider the fading effect of Image Plates, which causes the signal that will be measured by the reader to fall over time after the plate has been exposed. For this reason all the image plates used in the experiment are scanned at similar times after the laser shot has taken place. Direct exposure of image plate to visible light can also affect the data stored on IP, and is therefore carefully avoided [21].

3.5 References

- [1] M.H. Key et al., Physics of Plasmas, **14**, [2007].
- [2] M.H. Key et al., Journal of Physics, 1V, **133**, 371, [2006].
- [3] J.C. Fernandez et al., Nucl. Fusion, **49**, 065004, [2009].
- [4] T. Nakamura et al., Physical Review Letter, **93**, 265002, [2004].
- [5] A.P.L. Robinson, Physics of Plasmas, **14**, 083105, [2007].
- [6] P.A. Norreys, Nucl. Fusion, **49**, 104023, [2009].
- [7] J.A. King et al., Physics of plasmas, **16**, 020701, [2009].
- [8] M.H. Key et al., Central Laser Facility Annual Report, [2005/2006].
- [9] J.A. King et al., Physics of Plasmas, **16**, 2, [2009].
- [10] http://en.wikipedia.org/wiki/Vulcan_laser.
- [11] S.N. Chen et al., Physics of Plasmas, **14**, 102701, [2007].
- [12] A. Morace et al., Nuclear Instruments and Methods in Physics Research, **623**, 797-800, [2010].
- [13] K.U. Akli, Fast Ignition Experimental and Theoretical Studies, University of California Davis, [2006].
- [14] T. Lwasaki et al., Review of Scientific Instruments, **81**, [2010].

-
- [15] C. Gahn et al., Review of Scientific Instruments, **71**, 4, [2000].
- [16] D. Céolin et al., Review of Scientific Instruments, **81**, 063112, [2010].
- [17] H. Kato et al., Neurosurgical review, **8**, 53-62, [1985].
- [18] Y. Amemiya et al., Nature, **336**, 89-90, [1988].
- [19] K.A. Tanaka, Review of Scientific Instruments, **76**, 013507, [2005].
- [20]http://www.fujifilm.com/products/life_science/si_imgplate/img_plate.html.
- [21] L.W. Xi et al., *Sci China Ser G-Phys Mech Astron*, **51**, 10, [2008].
- [22] Y.T.Li et al, Physics Review Letters, **96**,165003, [2006].

Chapter 4

4.0 Results and analysis

In chapter 3 the use of a magnetic spectrometer to record electron emission from the laser interaction with a cone wire target was described. In this chapter the conversion of the recorded signals into electron spectra will be discussed, and these spectra will be analysed to gain some insight into the effect of defocussing the laser in such targets.

4.1 Data Analysis

When the IP scanner is employed to read the information stored on the image plate, an image file similar in appearance to that shown in figure 4.1 is produced.

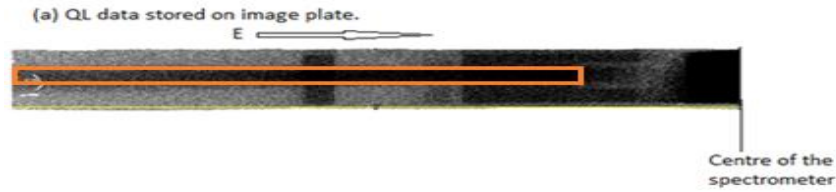


Figure 4.1. Shows the raw (QL) data stored on image plate. The red box indicates the region on the image plate where the electrons strike the image plate. Electrons with high energies have a smaller deflection angle whereas the electrons at low energies are deflected at a larger angle.

This data is converted into PSL (photo stimulated luminance) level by applying the formula given in Chapter 3. A lineout is then performed along the data contained in the signal region indicated in figure 4.1.

Distance (along x axis) is taken as number of pixels per unit length, which is converted into a unit of length by multiplying the number of pixels with 264.8mm, from a knowledge of the physical dimensions of the IP. The spectral dispersion in x can be obtained by using the analytical formula for the deflection of the electron in a circular, uniform magnetic field [1].

$$\tan \frac{\theta}{2} = \frac{r_b}{r_L}$$

Where r_L is the electron Larmor radius and r_b is the effective radius of the magnetised region, hence:

$$\tan \frac{\theta}{2} = \frac{eB_{\max}r_b}{|p|}$$

Where B_{\max} is the value of the magnetic field used in the spectrometer which is known on the basis of the instrument settings used in the experiment and previous measurements of the magnetic field vs. current relationship for the diagnostic. Knowing the deflection angle θ , the location at which the electrons of a particular energy will arrive at the IP can be determined from knowledge of the geometry of the spectrometer housing.

X-rays, gamma rays and electron with very high energies pass straight along the spectrometer axis and form a highly exposed “straight-through” signal on the IP. Electrons with lower energies deviate substantially from the straight line path under the influence of the magnetic field and hit the image plate at a location corresponding to their energy. Previous investigations have shown that, for these particular image plates, 1PSL corresponds to approximately 50 electrons.

The software Image-J is used for analysing the data. An important factor which should be considered while taking the lineout data along the image plate is the background signal level. As can be seen from figure 4.1, the background signal level is highly non-uniform due to a range of high energy radiations penetrating the spectrometer housing and exposing the IP directly. The structure of the spectrometer housing is non-uniform, when projected against the IP, so the background presented presents substantial spatial variability. Therefore a careful background subtraction must be performed as a first step in the analysis.

Following the extraction of the electron spectra as described above, the high energy tail of the distribution (such as is visible above the background noise) is then fitted

to a relativistic Maxwellian energy distribution function of some temperature T . At relativistic velocities the distribution of particles takes on a form described by the Maxwell-Juttner relationship:

$$f(\gamma) = \frac{\gamma^2 \beta}{\theta K_2(1/\theta)} \exp\left(-\frac{\gamma}{\theta}\right)$$

Where $\beta = v/c$, $\theta = kT/mc^2$, γ is the Lorentz factor and K_2 is a modified Bessel function of the second kind. This relationship allows for the fact that electrons gain mass as they approach the speed of light, c , and that their velocity cannot exceed c .

We then correlate the slope temperature obtained from the data to the extent of the laser defocus. In what follows the convention that we will use in describing the focus position is that -ve defocus refers to the laser reaching a focus within the cone, +ve defocus, conversely refers to the laser reaching a virtual focus beyond the cone tip (e.g. at some point along the wire). The displacement of focus is always along the axis of symmetry of the cone, and is measured from the inner surface of the cone tip. Furthermore, since the laser energy was quite variable from shot to shot, we have labelled our results according to whether they represent high energy shots, with an energy in the range 600 - 670 J, medium energy shots, with an energy in the range 540 - 600 J, or low energy shots with energies between 480 and 540 J.

4.2 Results

Below we show the fitted data for every shot in which analysable data was obtained. In each case, linear regression analysis is employed to fit the "best fit"

temperature to data. The other two curves, representing the highest and lowest temperatures that seem compatible with the data, are adjusted by eye according to the judgement of the author.

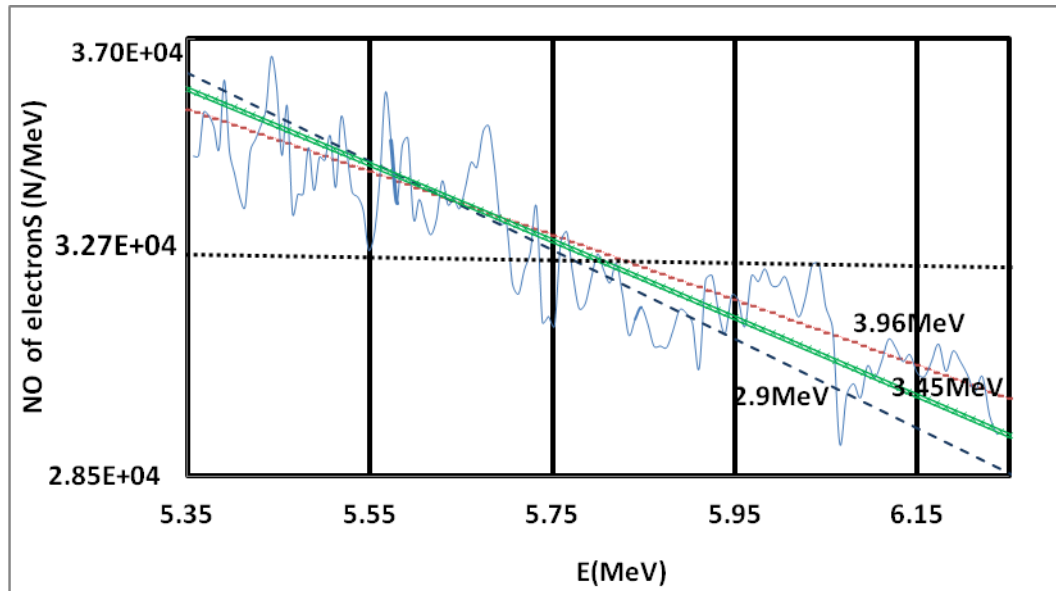


Figure 4.2. Relativistic Maxwellian fits to the data from a cone-wire target in tight focus. The best fit temperature was 3.45MeV. The energy for this shot was 579.0J (medium energy shot).

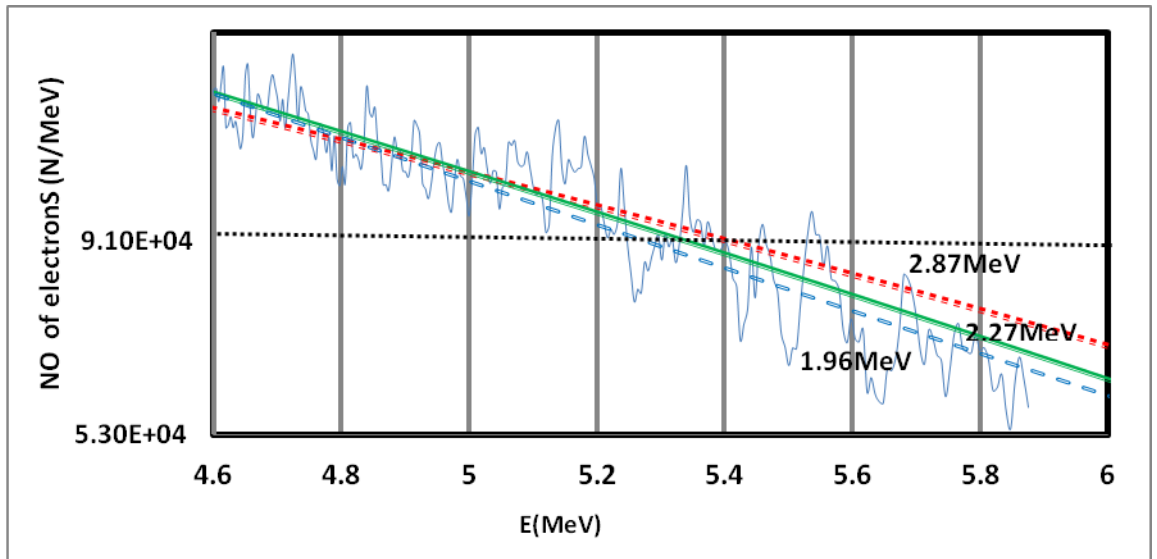


Figure 4.3. Relativistic Maxwellian fits to the data from a cone-wire target with the laser in tight focus at the tip. The best fit temperature was 2.27MeV. The incident energy for this shot was 564.4J (medium energy shot).

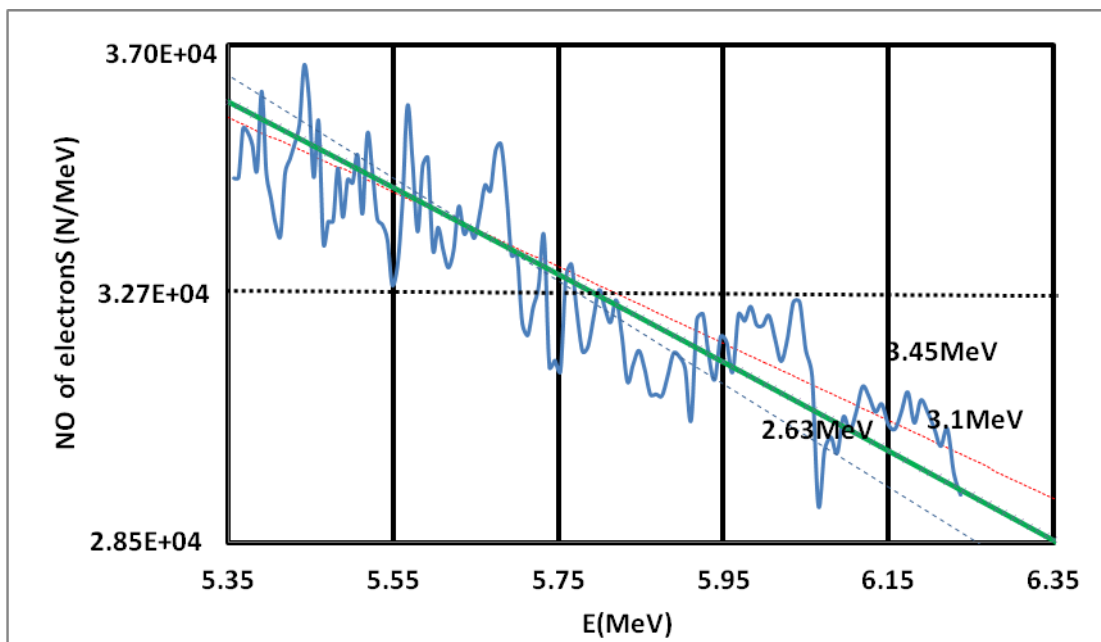


Figure 4.4. Relativistic Maxwellian fits to the data from a cone-wire target with the laser in tight focus at the tip. The best fit temperature was 3.1MeV. The incident energy for this shot was 628.2J (high energy shot).

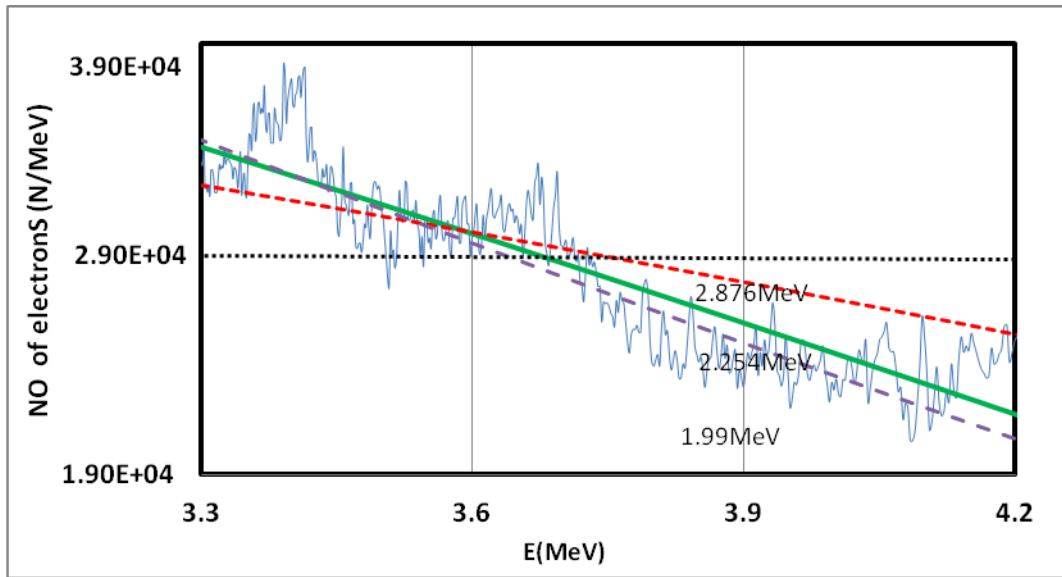


Figure 4.5. Relativistic Maxwellian fits to the data from a cone-wire target with the laser focussed 800 μ m before the tip. The best fit temperature was 2.254MeV. The incident energy for this shot was 660J (high energy shot).

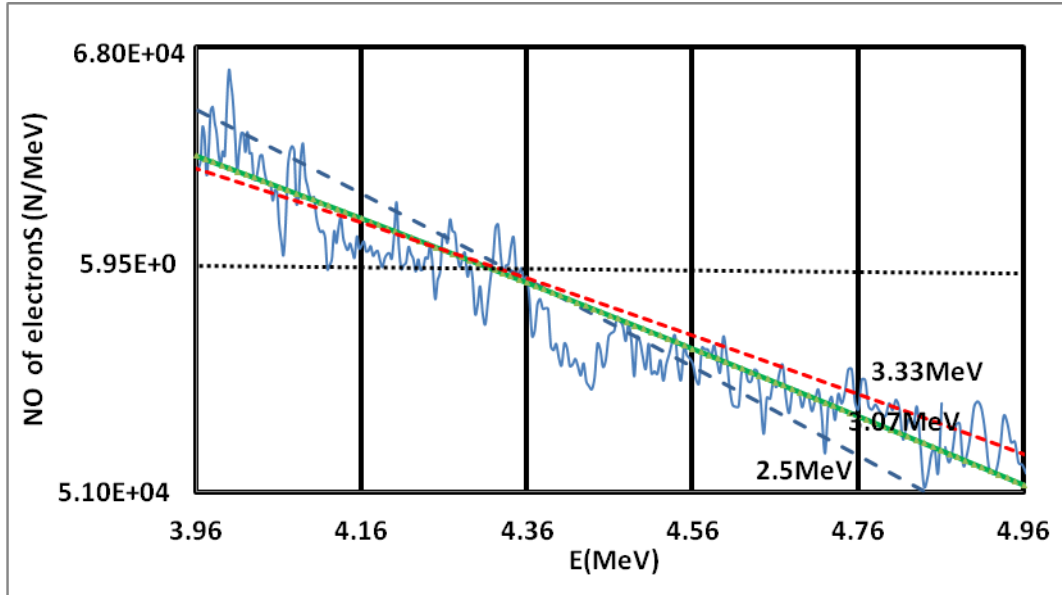


Figure 4.6. Relativistic Maxwellian fits to the data from a cone-wire target with the laser focussed 600 μ m before the tip. The best fit temperature was 3.07MeV. The incident energy for this shot was 54.8J (medium energy shot).

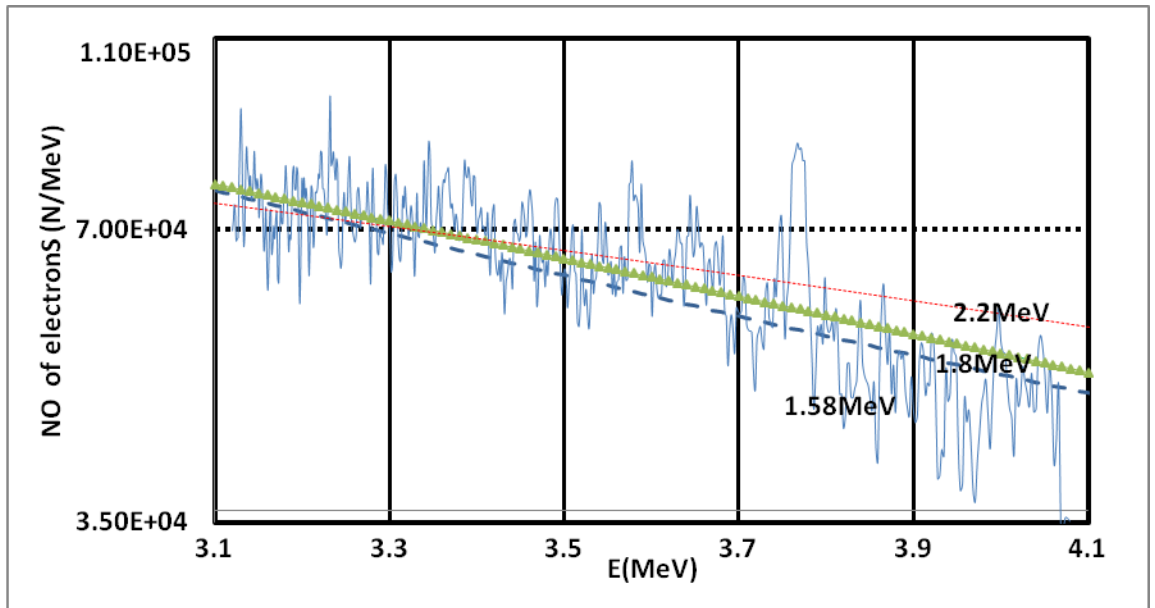


Figure 4.7. Relativistic Maxwellian fits to the data from a cone-wire target with the laser focussed 600 μ m before the tip.. The best fit temperature was 1.8MeV. The incident energy for this shot was 484.8J (low energy shot).

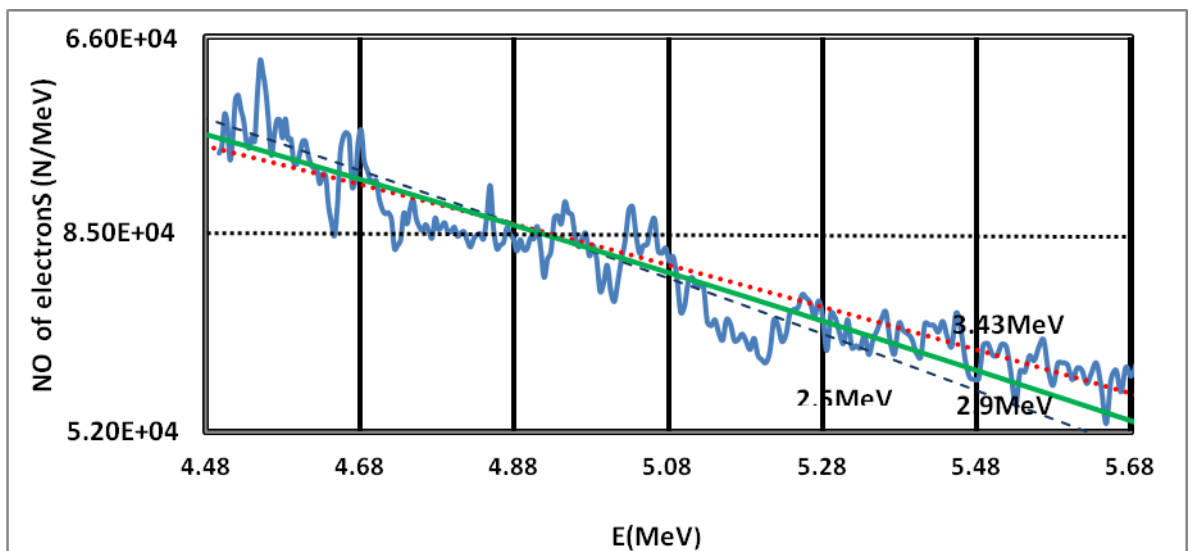


Figure 4.8. Relativistic Maxwellian fits to the data from a cone-wire target with the laser focussed 400 μ m before the tip.. The best fit temperature was 3.07MeV. The incident energy for this shot was 509.8J (low energy shot).

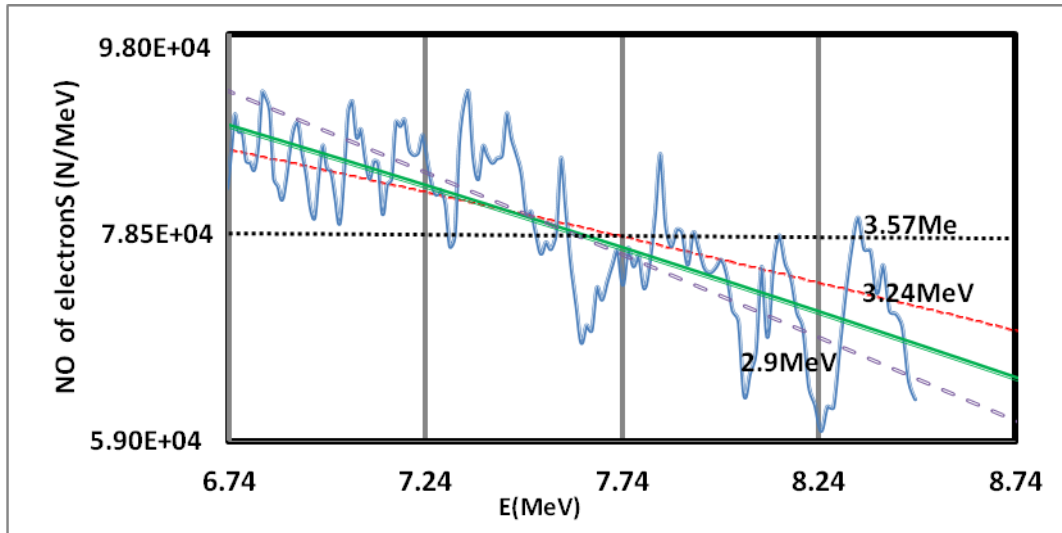


Figure 4.9. Relativistic Maxwellian fits to the data from a cone-wire target with the laser focussed 400 μ m before the tip.. The best fit temperature was 3.24MeV. The incident energy for this shot was 612.4J (high energy shot).

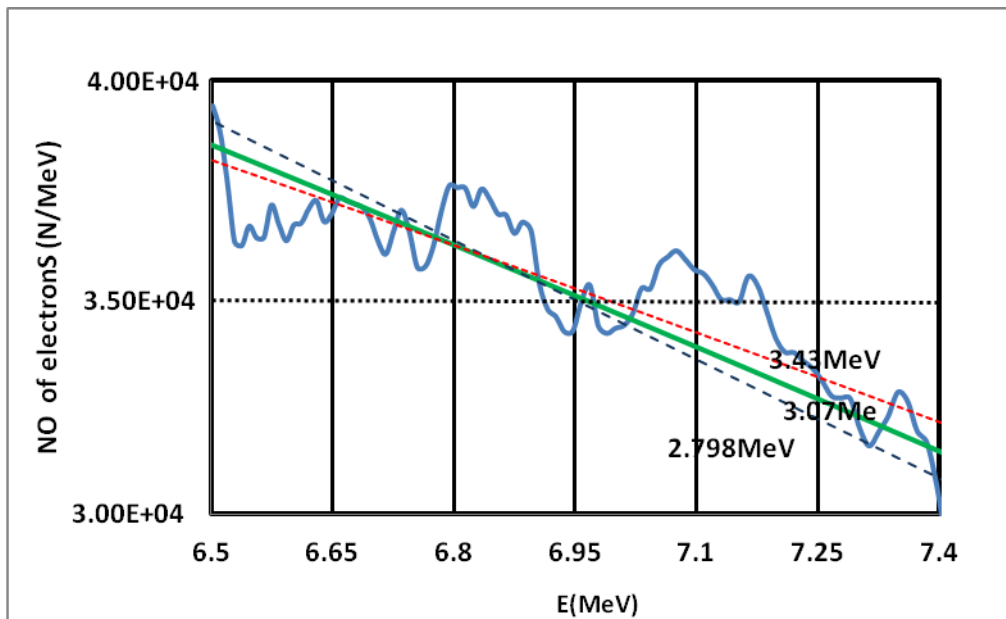


Figure 4.10. Relativistic Maxwellian fits to the data from a cone-wire target with the laser focussed 200 μ m before the tip. The best fit temperature was 3.07MeV. The incident energy for this shot was 600J (high energy shot).

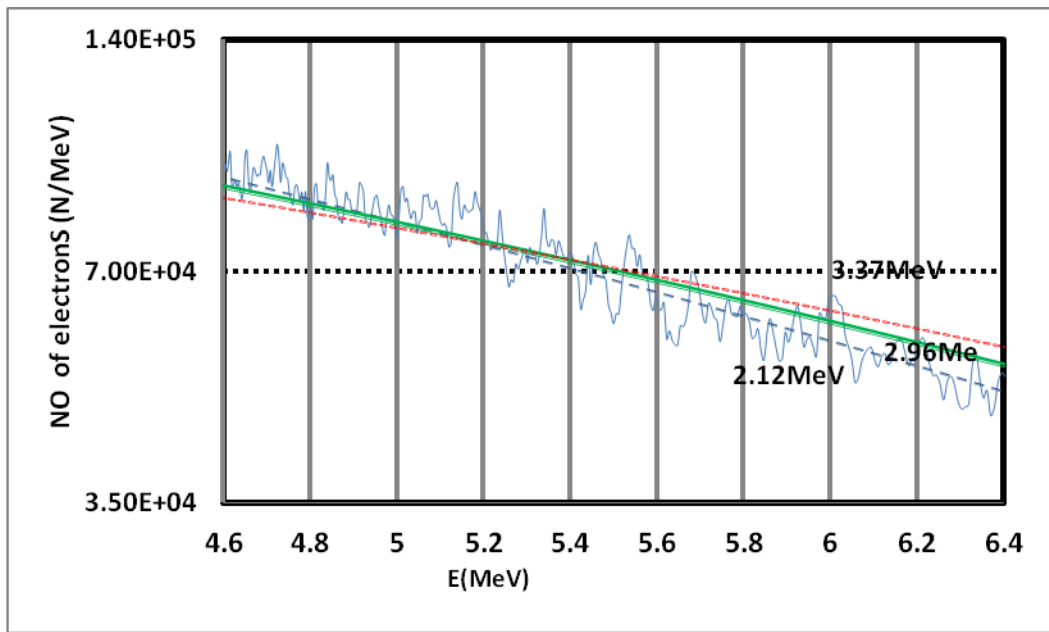
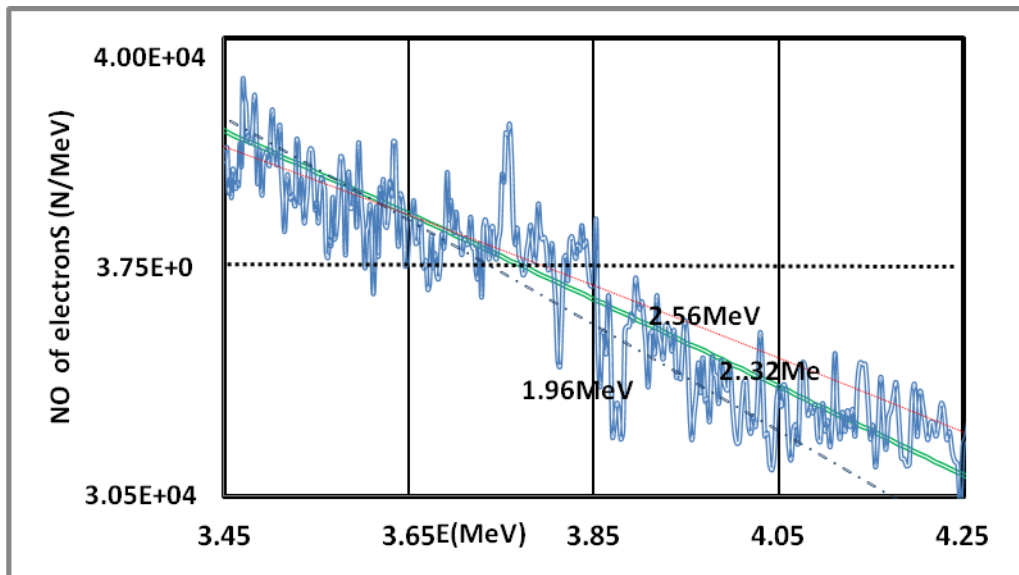


Figure 4.11. Relativistic Maxwellian fits to the data from a cone-wire target with the laser focused 200 μ m before the tip. The best fit temperature was 2.96MeV. The incident energy for this shot was 486.7J (low energy shot).



Figure

4.12. Relativistic Maxwellian fits to the data from a cone-wire target with the laser focused 100 μ m before the tip. The best fit temperature was 2.32MeV. The incident energy for this shot was 595.4J (medium energy shot).

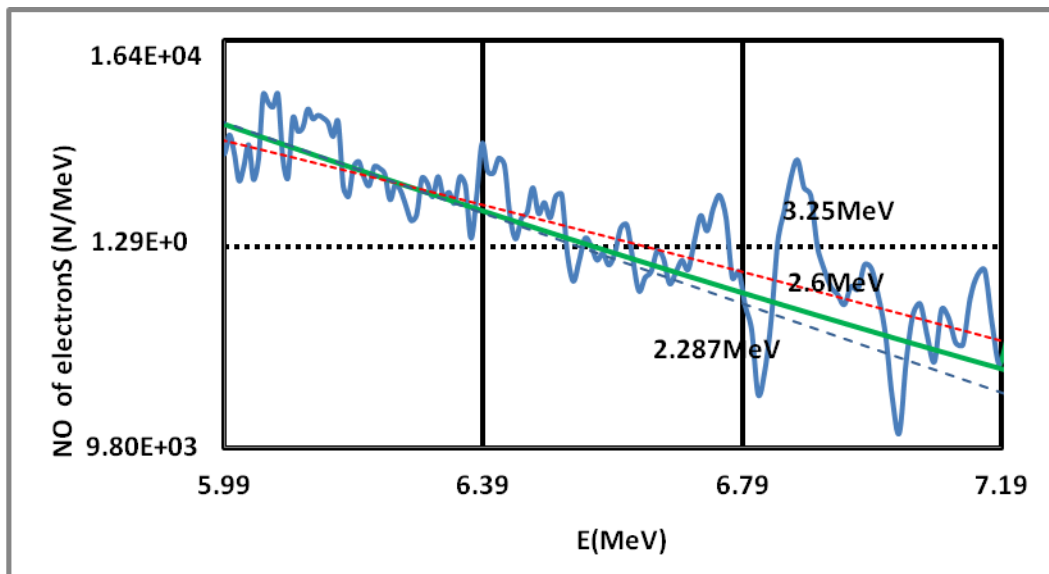


Figure 4.13. Relativistic Maxwellian fits to the data from a cone-wire target with the laser focussed 100 μ m before the tip.. The best fit temperature was 2.6MeV. The incident energy for this shot was 665.6J (high energy shot).

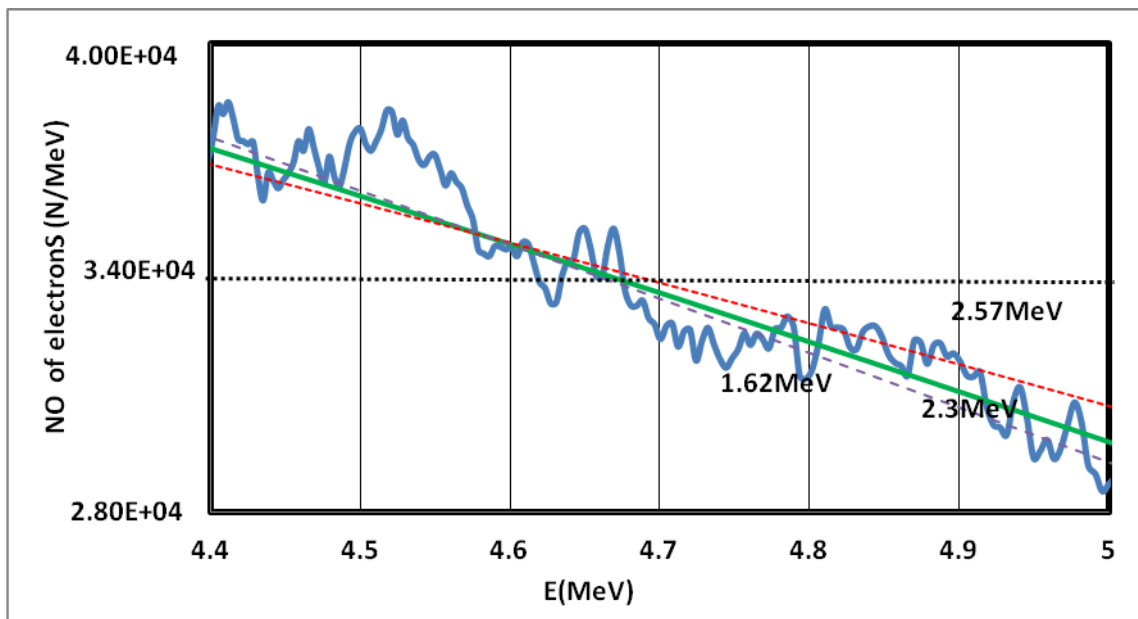


Figure 4.14. Relativistic Maxwellian fits to the data from a cone-wire target with the laser focussed 100 μ m past the tip. The best fit temperature was 2.3MeV. The incident energy for this shot was 541.8J (medium energy shot).

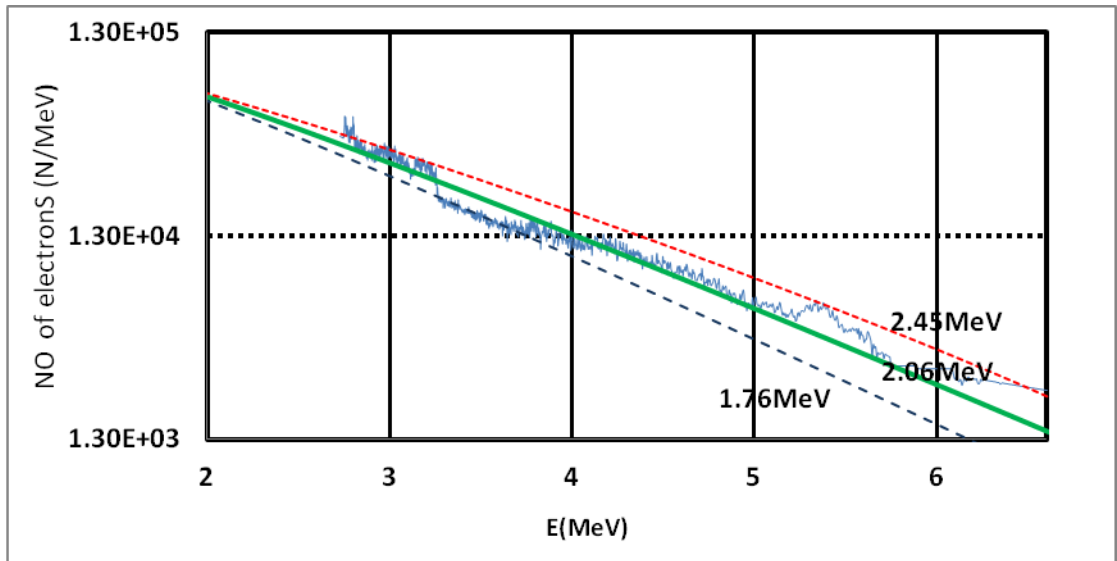


Figure 4.15. Relativistic Maxwellian fits to the data from a cone-wire target with the laser focussed $400\mu\text{m}$ past the tip. The best fit temperature was 2.06MeV . The incident energy for this shot was 608J (medium energy shot).

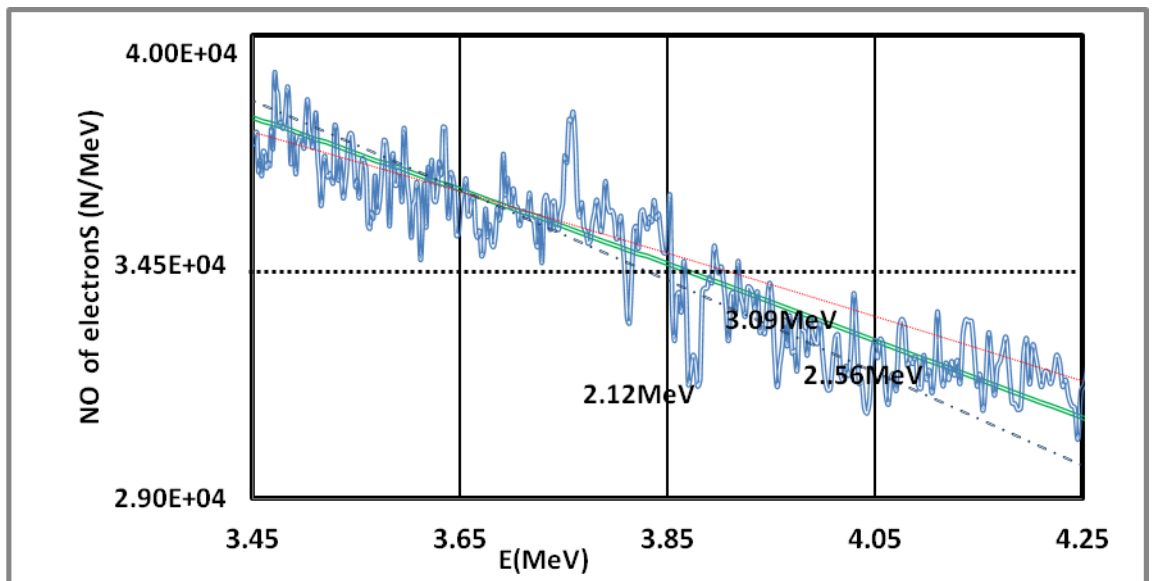


Figure 4.16. Relativistic Maxwellian fits to the data from a cone-wire target with the laser focussed $400\mu\text{m}$ past the tip. The best fit temperature was 2.56MeV . The incident energy for this shot was 561J (high energy shot).

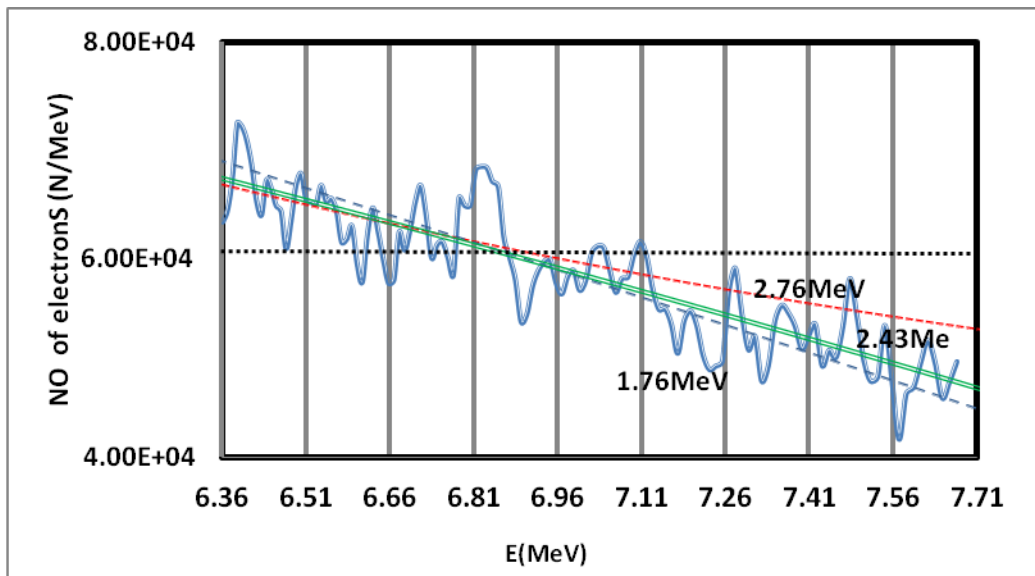


Figure 4.17. Relativistic Maxwellian fits to the data from a cone-wire target with the laser focussed 600 μ m past the tip. The best fit temperature was 2.43MeV. The incident energy for this shot was 533J (low energy shot).

4.3 Summary of results

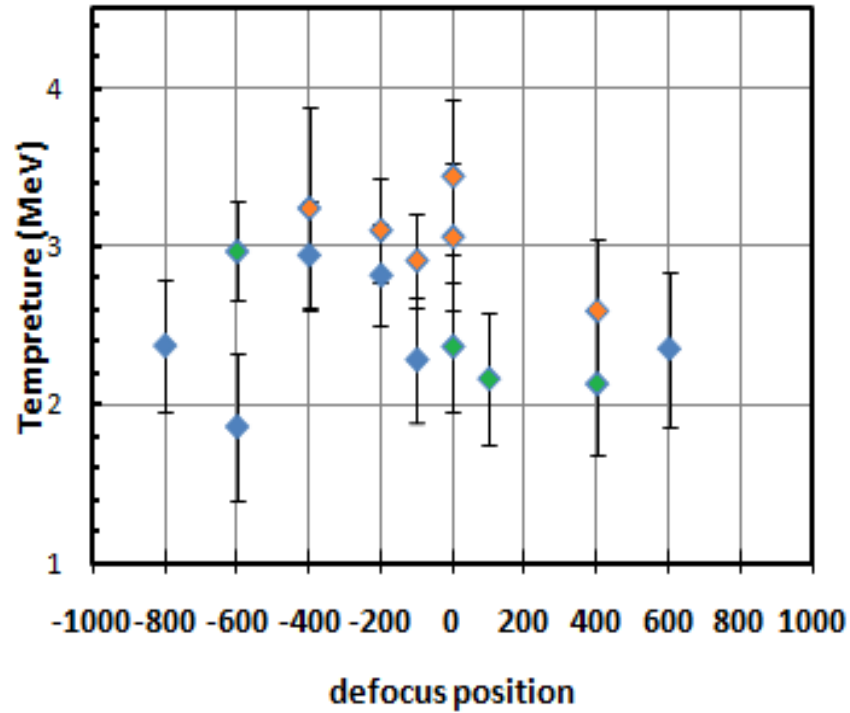


Figure 4.18. Hot electron slope temperatures taken from electron spectroscopy measurements made during shots onto cone-wire targets with varying degrees of defocus. Low (blue), medium (green) and high (red) refer to laser shot energies of 480 - 540 J, 540 - 600 J and 600 - 670 J respectively.

Figure 4.18 shows the slope temperatures associated with the varying degrees of defocus employed in the experiment. The temperature of the hot electron spectrum does not appear to follow any strong trend with defocussing, however, as expected, the highest energy shots do appear to correlate with somewhat higher slope temperatures.

In previous studies it has been seen that the variation in hot electrons temperatures is a function of laser intensity [2], however it is not trivial to relate the focus position to the incident intensity at the target surface, since the cone acts, in part, to focus the incident laser radiation toward the cone tip. More extensive analysis on this experiment has been performed by Ian Bush, who has used the 1/e length of the K- α emission from the wire portion of the targets as an indicator of the temperature of the hot electron population within the target. A plot of these results is shown in figure 4.19.

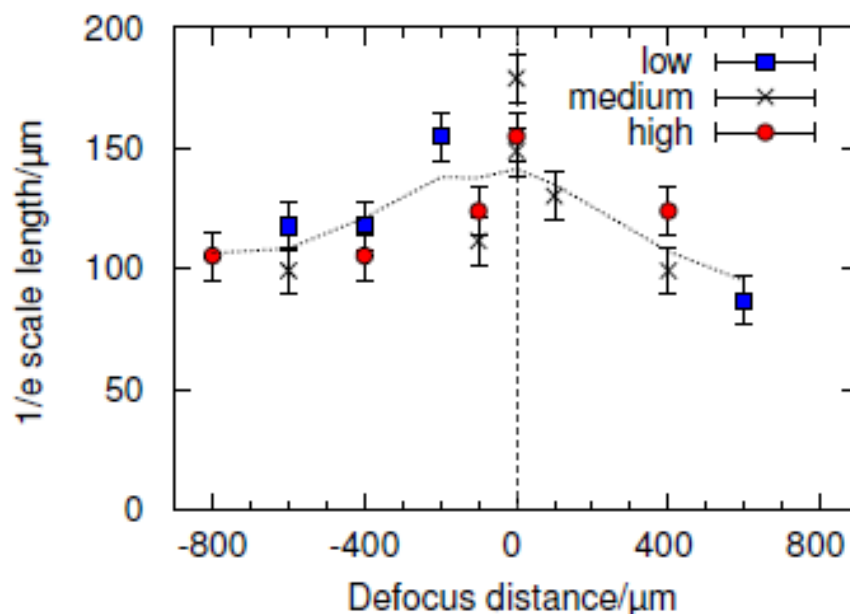


Figure 4.19. Variation of the length over which the K α emission falls to 1/e of its peak value in the same.

As can be seen from figure 4.19, the change in the 1/e length of the fluorescent emission from the copper wire seems to suggest that the spectrum of the hot electrons within the target is a function of focus position, with the hotter spectra

being present around tight focus, as might be expected based upon the dependence of the hot temperature upon the intensity.

This suggests that the spectrum recorded at a distance from the target may not be representative of the hot electron spectrum present within the target. This is in fact an understood limitation of electron spectroscopy diagnostics at a distance from the target, and is the reason why the more difficult to setup $k\text{-}\alpha$ diagnostics were deployed for this purpose. The difference in spectra measured at a distance is caused by the strong electromagnetic sheath fields that surround the dense target. These fields tend to trap all but the most energetic electrons from leaving the target, and furthermore they tend to reduce the energy of those electrons that do escape to infinity. However, as should be clear from a consideration of figures 4.18 and 4.19, the electron spectroscopy results presented in this thesis do not contradict the findings of the $k\text{-}\alpha$ diagnostics. This is encouraging, and provides limited support for the broader conclusions of the study, which will be described in detail in the PhD thesis of Mr Ian Bush (under preparation).

The results of the $k\text{-}\alpha$ diagnostics further suggest that the coupling efficiency to energetic electrons is maintained throughout the defocus range tested in this experiment. This is indeed an interesting result since fast ignition would be made far more practicable if the electron spectrum could be softened whilst maintaining energy coupling efficiency to the core. However caution must be exercised in extending the results of this study at laser energies of a few hundred Joules, and $\sim 1\text{ps}$ pulse lengths, to conditions typical of fast ignition for which laser energies on

the order of 100kJ and pulse durations of approximately 10-20ps are thought to be required.

4.4 References

- [1] G.E. Uhlenbeck and L.A. Young , Physics Review Letters, **36**, 1721-1727
,[1930].
- [2] F.N. Beg et al., Physics of Plasmas, **4**, 447, [1997].

Chapter 5

5.0 Conclusions

Fast ignition is an interesting variant upon the inertial confinement fusion scheme which offers the promise of high gain laser fusion without the requirement for exorbitantly expensive multi-MJ laser drivers. A major problem difficulty with the scheme is that the ignition hotspot must be formed in a region of constant density. This results in a hotspot that is at a far higher pressure than the surrounding fuel, causing it to disassemble rapidly. Therefore the heating energy must be supplied in a very short period of time ($\sim 10\text{ps}$). This dictates that a very high laser intensity is required. However at the intensities suggested ($\sim 10^{21}\text{W/cm}^2$) the relativistic electrons produced by the laser interaction with the target are too energetic to be stopped in a λ comparable to the minimum required for ignition. This implies that the ignition process will then require far more energy, since a far greater mass of fuel must be heated.

For this reason it would be highly desirable to produce a softer electron spectrum with a given igniter laser [1]. A number of approaches to achieving this

have been suggested, such as operating at a shorter wavelength or using plasma mirrors. However all of these approaches have clearly apparent difficulties of their own.

The results of the experiment performed at the Vulcan Petawatt laser in Nov/Dec 2008, which are in part outlined in this thesis, suggest that defocussing the laser that is incident into the cone, in the cone-guided approach to fast ignition, may enable the electron spectrum to be softened whilst the laser-target coupling efficiency is approximately maintained. However great caution must be exercised in extrapolating the results of this study, which was carried out with a laser of ~ 1 ps duration and energy ~ 600 J to a full scale fast ignition driver which would likely have an energy on the order of 100kJ and a duration of 10-20ps.

The electron spectroscopy results presented in this thesis are less convincing in showing a reduction in the hot electron temperature with defocus than are those based upon observations of $k\text{-}\beta$ emission from the wire. One explanation for this is that the spectrum at a distance from the target is in large part a function of the electromagnetic sheath fields that surround the target, and is only weakly dependent upon the spectrum of electrons in the dense plasma.

5.1 References

- [1] B. Chrisma, Phys of plasma , 15, 056309 2008
